Research Square

Preprints are preliminary reports that have not undergone peer review.
They should not be considered conclusive, used to inform clinical practice,
or referenced by the media as validated information.

Strain-mediated degradation and contact-guided deposition can explain collagen organization in healthy and infarcted myocardium

L.H.F. Souren
Eindhoven University of Technology
H. Hoursan
Eindhoven University of Technology
K.L.P.M. Janssens
Eindhoven University of Technology
P.H.M. Bovendeerd
Eindhoven University of Technology
T. Ristori
Eindhoven University of Technology
C.V.C. Bouten
Eindhoven University of Technology
S. Loerakker
s.loerakker@tue.nl
Eindhoven University of Technology

Research Article

Keywords: collagen organization, left ventricular alignment, strain-dependent collagen degradation, cardiac fibroblasts, multiscale modeling, contact guidance

Posted Date: November 9th, 2026

DOI: https://doi.org/10.21203/rs.3.rs-11405289/v1

License: This work is licensed under a Creative Commons Attribution 4.0 International License.
Read Full License

Additional Declarations: No competing interests reported.

Strain-mediated degradation and contact-guided deposition can explain collagen organization in healthy and infarcted myocardium

L.H.F. Souren[1,2†], H. Hoursan[1,2†], K.L.P.M. Janssens[1], P.H.M. Bovendeerd[1], T. Ristori[1,2], C.V.C. Bouten[1,2†], S. Loerakker[1,2*†]

[1]Department of Biomedical Engineering, Eindhoven University of Technology, Eindhoven, 5600 MB, The Netherlands.
[2]Institute for Complex Molecular Systems (ICMS), Eindhoven, 5600 MB, The Netherlands.

*Corresponding author(s). E-mail(s): s.loerakker@tue.nl;
†L.H.F. Souren and H. Hoursan contributed equally to this work and share first authorship. C.V.C. Bouten and S. Loerakker contributed equally to this work and share last authorship.

Abstract

Understanding mechanobiology-driven cardiac collagen organization is crucial for devising strategies to restore tissue structure and function of diseased hearts. Here, we developed a computational framework that couples a mechanics model of the left ventricle with a mechanobiology-informed model of collagen reorientation to investigate the mechanisms underlying cardiac collagen organization. The framework could replicate physiological left ventricular collagen orientation only when assuming that collagen degradation follows a V-shaped relation with strain. Furthermore, contact guidance between cardiac fibroblasts and collagen fibers emerged as an important mechanism for maintaining collagen orientation and anisotropy. Being aligned with the collagen fibers, cardiac fibroblasts promoted strong collagen anisotropy through deposition in the main direction of the cell. In contrast, increased fibroblast contractility resulted in unphysiological orientations of the cells and therefore misaligned collagen deposition. This suggests that fibroblasts maintain rather than drive the collagen orientation in the healthy heart. In the infarcted left ventricle, however, the same mechanobiological mechanisms that explain physiological collagen organization lead to reorientation of the collagen fibers and reduced anisotropy, which is consistent with literature observations. These findings may contribute to the design of novel targeted therapeutic strategies aimed at restoring myocardial structure-function relationships in diseased hearts.

Keywords: collagen organization, left ventricular alignment, strain-dependent collagen degradation, cardiac fibroblasts, multiscale modeling, contact guidance

1 Introduction

The alignment of collagen fibers in the myocardium is a crucial determinant of the heart's mechanical function. Arranged in opposing helices across the left ventricular wall, the myocardial collagen network supports passive cardiac mechanics and force transmission while preventing cardiomyocyte slippage and overstretching (Pope et al. 2008; Spinale 2007; Weber et al. 1994). The interaction between this highly organized architecture and active cardiomyocyte contraction creates a unique mechanical environment characterized by cyclic multiaxial deformations. Remarkably, despite continuous collagen fiber turnover mediated by cardiac fibroblast cells (Weber 1989), the orientation and anisotropy of the myocardial collagen network are well maintained throughout adult life (Humphrey and Rajagopal 2002). How the orientation and anisotropy of this highly organized collagen architecture are maintained during continuous collagen turnover within the demanding mechanical environment of the beating heart remains incompletely understood.

It is known that mechanobiological mechanisms must play a critical role in maintaining the physiological cardiac collagen architecture. The importance of mechanobiological mechanisms is revealed in pathological conditions, where alterations in myocardial mechanical loading conditions lead to adverse structural remodeling of the collagen network (Fomovsky et al. 2012; Spinale 2007; Weber 1989). Such remodeling is characterized by an excessive deposition of newly synthesized collagen fibers (fibrosis) and disturbances in collagen fiber alignment, leading to altered (an)isotropic tissue properties. While the regulation of myocardial collagen amount in health and disease is increasingly well understood (Braidotti et al. 2024; Brilla et al. 1995; Weber and Brilla 1991; Younesi et al. 2024), substantially less is known about the mechanobiological mechanisms that regulate cardiac collagen fiber orientation and tissue anisotropy. Identifying these mechanisms and their interplay may reveal opportunities to prevent, halt, or therapeutically reverse structural disorganization in cardiac disease.

Numerous *in vitro* studies have identified mechanobiological mechanisms underlying the regulation of collagen fiber orientation in soft tissues. One mechanism by which collagen orientation can be controlled is strain-dependent collagen degradation. Mechanical strain can influence the targeted binding of degradative enzymes to collagen fibers, resulting in direction-dependent degradation and changes in tissue anisotropy (Ghazanfari et al. 2016; Huang and Yannas 1977; Wyatt et al. 2009; Yeganegi et al. 2023). Besides strain-dependent degradation, collagen-producing stromal cells, such as cardiac fibroblasts, can influence collagen orientation through directional collagen synthesis (Bai et al. 2014; Bishop 1998; Nguyen et al. 2009) and fiber prestretch (Atluri et al. 2020; Meshel et al. 2005). Consequently, understanding cardiac collagen orientation also requires consideration of the mechanisms governing fibroblast orientation. Fibroblasts have been shown to reorient in response to local mechanical and structural cues, including substrate stiffness (Saez et al. 2007), cyclic strain (strain avoidance) (Foolen et al. 2012; Gould et al. 2012; Mostert et al. 2022; Wang and Grood 2000), and extracellular matrix architecture (contact guidance) (Guido and Tranquillo 1993; de Jonge et al. 2013; Wang and Grood 2000), which together determine the direction and magnitude of cellular traction forces on their surroundings.

The complex interplay between *in vivo* tissue mechanics and experimentally established mechanobiological mechanisms determining collagen organization is best studied using *in silico* modeling. For example, in paediatric heart valves, a continuum mechanics model revealed that cellular forces and (re)orientation in response to mechanical stimuli are critical for the emergence of functional collagen orientation, while cellular contact guidance from the surrounding collagen is required to maintain this organization (Ristori et al. 2018a). Furthermore, agent-based models incorporating fibroblast-mediated collagen (re)orientation mechanisms successfully reproduced collagen alignment and anisotropy in healing tendons (Richardson et al. 2018) and infarcted myocardium (Fomovsky et al. 2012; Rouillard and Holmes 2014; Zhuan et al. 2019), while identifying local strain anisotropy as an important regulator of collagen organization.

In the beating left ventricle, *in silico* modeling has been applied to demonstrate the strong influence of local mechanical stimuli on physiological and pathological myocardial tissue orientation

(Arts et al. 1994; Kroon et al. 2009; Mehri and Wenk 2026; Mehri et al. 2024, 2025; Washio et al. 2016, 2020). Across a range of proposed driving stimuli, including active stress and shear along cardiomyocyte fiber bundles, these models consistently predict fiber reorientation toward architectures associated with improved left ventricular function and homogenized loading conditions along the fiber direction. However, the biological mechanisms through which such mechanical cues drive myocardial structural reorientation were not the focus of these studies. The experimental and *in silico* studies in other soft tissues suggest that mechanobiological regulation of collagen organization may provide a biological link between local mechanical stimuli and myocardial tissue orientation. Whether these mechanisms also contribute to the establishment and maintenance of myocardial architecture in the beating left ventricle remains largely unexplored.

Therefore, the aim of the present study is to investigate whether, and if so to what extent, the previously described mechanobiological mechanisms are crucial for regulating physiological collagen organization in the ever-beating, complex mechanical environment of the left ventricle. To address this, we developed a computational framework that couples an established finite element model for calculating local left ventricular deformations (Janssens et al. 2023) to a mechanobiology-motivated collagen (re)orientation model (Ristori et al. 2018a). Additionally, we applied the framework to simulate an infarcted left ventricle with the aim of determining whether the same mechanobiological mechanisms that maintain physiological cardiac collagen architecture also explain the structural (dis)organization in a pathological case.

2 Methods

2.1 Finite element model of the left ventricle

A previously developed finite element (FE) model was used to obtain spatiotemporal deformation profiles throughout the left ventricular wall (Bovendeerd et al. 2009; Janssens et al. 2023). The model implementation and parameter values were adopted from these studies without modification, and only a brief description is provided here.

A generalized, truncated ellipsoidal geometry was modeled to represent a human-like left ventricle (Figure 1a). The Cauchy stress tensor in the left ventricle was decomposed into passive and active material behavior

$$\boldsymbol{\sigma}_{\mathrm{LV}} = f_{\mathrm{pas}}\boldsymbol{\sigma}_{\mathrm{pas}} + f_{\mathrm{act}}\boldsymbol{\sigma}_{\mathrm{act}} \qquad (1),$$

where f_{pas} and f_{act} are multiplication scalars that allow for spatial variations in material properties in the left ventricle. For the healthy left ventricle, both these parameters were set to 1. Passive material stress, $\boldsymbol{\sigma}_{\mathrm{pas}}$, was described via a Fung-type hyperelastic material model accounting for nonlinearly elastic, transversely isotropic and nearly incompressible material behavior. The material model for sarcomere active contraction, $\boldsymbol{\sigma}_{\mathrm{act}}$, accounted for the time-, length-, and velocity-dependent relations. A rule-based myofiber architecture was used to define the anisotropic material behavior of both $\boldsymbol{\sigma}_{\mathrm{pas}}$ and $\boldsymbol{\sigma}_{\mathrm{act}}$. Fiber orientations varied transmurally from a right-handed endocardial orientation (helix angle $\alpha_{\mathrm{h}}^{\mathrm{ref}} \approx +70°$), through a more circumferential midwall orientation ($\alpha_{\mathrm{h}}^{\mathrm{ref}} \approx 20°$), to a left-handed epicardial orientation ($\alpha_{\mathrm{h}}^{\mathrm{ref}} \approx -50°$). A detailed description of the fiber field parametrization is provided in Supplementary A.1.

Boundary conditions were applied at the base and endocardial surface. At the base, longitudinal displacements were fixed and the remaining rigid-body translations and rotations were suppressed. The endocardial surface was subjected to a uniform cavity pressure, determined from mechanical equilibrium during the isovolumetric phases and from coupling to a 0D closed-loop circulatory model during filling and ejection. A heart rate of 75 beats per minute was prescribed, corresponding to a cardiac cycle period of $T = 0.8$ [s].

The diseased left ventricle model featured a transmural, tear-shaped infarct region spanning from the equator to the apex, representative of an occlusion of the left anterior descending (LAD) artery (Janssens et al. 2023). Infarct properties differed from physiological myocardium properties by neglecting any active contraction in the infarct ($f_{\mathrm{act}} = 0$) and by stiffening of the passive material properties ($f_{\mathrm{pas}} = 10$) representative of chronic infarction. Lastly, a 5 mm wide region surrounding the infarct was modeled as the border

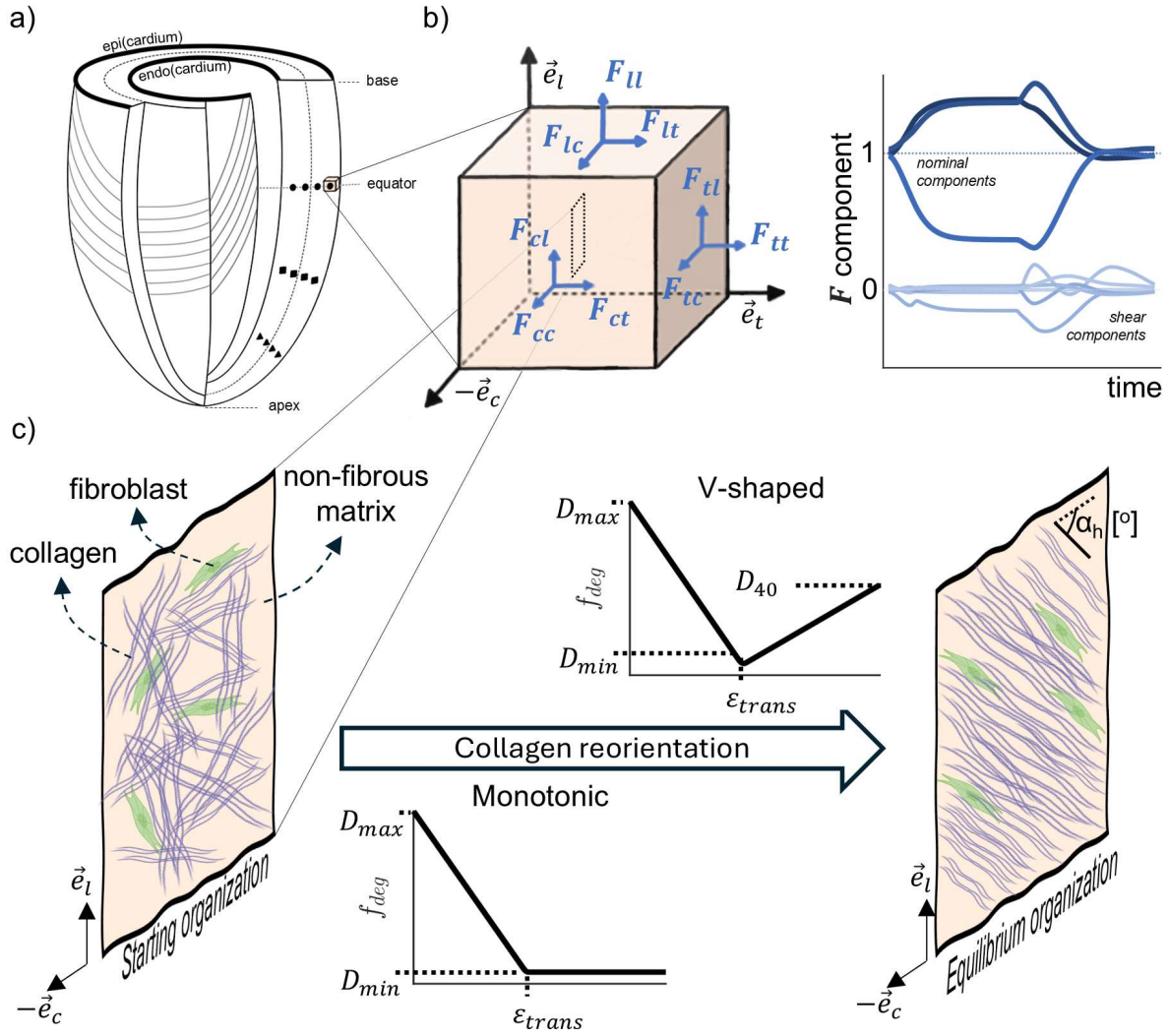


Fig. 1 Schematic representation of the computational framework. a) FE model of the left ventricle, indicating the locations from which cyclic spatiotemporal deformation profiles were extracted. b), c) Overview of the mechano-mediated collagen reorientation methodology. b) A single, linearly interpolated hexahedral element was subjected to the deformation profiles extracted from the FE simulation, thereby reproducing the local mechanical environment of the left ventricular wall. c) Collagen reorientation in the circumferential-longitudinal plane is illustrated. Starting from an isotropic organization, collagen reorientation over time resulted in an aligned equilibrium organization. Two strain-mediated collagen degradation hypotheses were evaluated: V-shaped and monotonic. $D_{\max}$ and $D_{\min}$ are the maximum and minimum normalized degradation rates, respectively. D_{40} is the normalized degradation rate at $\varepsilon_e = 0.40$ [-]. c) was created with BioRender.com

zone, with f_{pas} and f_{act} linearly varying between the physiological and infarcted values. Simulations were performed using the FEniCS open-source computing platform (Baratta et al. 2023).

2.2 Mechano-mediated fibroblast & collagen (re)orientation

A previously developed mechano-mediated model describing fibroblast-driven collagen fiber (re)orientation in heart valves and engineered *in vitro* tissues was applied to study collagen organization in the left ventricular mechanical environment (Loerakker et al. 2014; Obbink-Huizer et al. 2014; Ristori et al. 2018a,b). The material stress of the non-cardiomyocyte components in the myocardium was defined by

$$\boldsymbol{\sigma}_{\text{tissue}} = \boldsymbol{\sigma}_{\text{m}} + \boldsymbol{\sigma}_{\text{sf}} + \boldsymbol{\sigma}_{\text{cf}} \qquad (2),$$

with $\boldsymbol{\sigma}_{\text{m}}$ the Cauchy stress of the non-fibrous matrix constituents, $\boldsymbol{\sigma}_{\text{sf}}$ the stress of actin stress fibers in the cardiac fibroblasts and $\boldsymbol{\sigma}_{\text{cf}}$ the collagen fiber stress. Both stress fibers and collagen fibers were distributed by $N = 30$ discrete, independent fiber orientations spanning the circumferential-longitudinal plane with a resolution between each fiber direction of 6°. Each ith fiber direction in the reference configuration was described by $\boldsymbol{e}^i_{\text{f0}} = \cos(\gamma^i)\boldsymbol{e}_{\text{c}} + \sin(\gamma^i)\boldsymbol{e}_{\text{l}}$, with $\boldsymbol{e}_{\text{c}}$ and $\boldsymbol{e}_{\text{l}}$ the circumferential and longitudinal unit vector and γ^i the angle of $\boldsymbol{e}^i_{\text{f0}}$ with respect to $\boldsymbol{e}_{\text{c}}$.

2.2.1 Actin stress fibers in cardiac fibroblasts

The anisotropic stress contribution of actin stress fibers was modeled as

$$\boldsymbol{\sigma}_{\text{sf}} = \frac{1}{N}\sum_{i=1}^{N} \phi^{i,\text{p}}_{\text{sf}}\sigma^{i,\text{p}}_{\text{sf}}\boldsymbol{e}^i_{\text{f}}\boldsymbol{e}^i_{\text{f}} \qquad (3),$$

with $\boldsymbol{e}^i_{\text{f}}$ representing the unit vector $\boldsymbol{e}^i_{\text{f0}}$ in the current configuration, such that $\lambda^i_{\text{f}}\boldsymbol{e}^i_{\text{f}} = \boldsymbol{F}\cdot\boldsymbol{e}^i_{\text{f0}}$. Here, $\boldsymbol{F} = \frac{\partial \boldsymbol{x}}{\partial \boldsymbol{x}_0}$ is the deformation gradient tensor where $\boldsymbol{x}$ and $\boldsymbol{x}_0$ are material point coordinates in the deformed and undeformed reference configurations, respectively. From this, λ^i_{f}, which is the global stretch along direction i, can be determined via

$$\lambda^i_{\text{f}} = \sqrt{\boldsymbol{e}^i_{\text{f0}}\cdot\boldsymbol{F}^{\text{T}}\cdot\boldsymbol{F}\cdot\boldsymbol{e}^i_{\text{f0}}} \qquad (4).$$

Furthermore, $\phi^{i,\text{p}}_{\text{sf}}$ is the polymerized actin stress fiber volume fraction in direction i with corresponding stress magnitude $\sigma^{i,\text{p}}_{\text{sf}}$. For readability purposes, we will neglect the p superscript in the remainder of the equations. The total amount of actin $\phi^{\text{tot}}_{\text{sf}}$ remained constant and consisted of monomeric ($\phi^{\text{m}}_{\text{sf}}$) and polymerized actin

$$\phi^{\text{tot}}_{\text{sf}} = \phi^{\text{m}}_{\text{sf}} + \frac{1}{N}\sum_{i=1}^{N}\phi^i_{\text{sf}} \qquad (5),$$

with starting conditions $\phi^{\text{tot}}_{\text{sf}} = \phi^{\text{m}}_{\text{sf}}$. The stress magnitude was defined as

$$\sigma^i_{\text{sf}} = \sigma_{\max} f_\varepsilon(\varepsilon^i) f_{\dot\varepsilon}(\dot\varepsilon^i) \qquad (6),$$

with $\sigma_{\max}$ the maximum stress fiber contraction and $\varepsilon^i = 0.5((\lambda^i_{\text{f}})^2 - 1)$ the strain in fiber direction i as derived from the Green-Lagrange strain tensor. The dependence of stress fiber passive and active contraction stress on strain, $f_\varepsilon(\varepsilon^i)$, and strain rate, $f_{\dot\varepsilon}(\dot\varepsilon^i)$, are described elsewhere (Obbink-Huizer et al. 2014) (Suppl. A.2).

The mechanoregulated (re)orientation of polymerized stress fibers depended on strain, strain-rate, and structural contact-guidance provided by adjacent collagen fibers.

$$\begin{aligned}\frac{\text{d}\phi^i_{\text{sf}}}{\text{d}t} = (k^{\text{f}}_0 + k^{\text{f}}_1\sigma_{\max} f_{\varepsilon,\text{a}}(\varepsilon^i) f_{\dot\varepsilon}(\dot\varepsilon^i) \\ + f_{\text{cg}}(\phi^i_{\text{cf}}))\phi^{\text{m}}_{\text{sf}} - k_{\text{d}}\phi^i_{\text{sf}}\end{aligned} \qquad (7),$$

where k^{f}_0 and k_{d} quantify basal stress fiber formation and degradation while k^{f}_1 scales with mechano-mediated stress fiber formation. The effect of contact guidance was modeled with a sigmoid function that scaled the contact guidance effect with the directional volume fraction of collagen fibers ϕ^i_{cf} (Ristori et al. 2018b)

$$f_{\text{cg}}(\phi^i_{\text{cf}}) = g_{\text{cg}}\left(1 - \frac{k^{\text{cg}}_1}{\text{e}^{k^{\text{cg}}_2\phi^i_{\text{cf}}} + k^{\text{cg}}_1 - 1}\right) \qquad (8),$$

where g_{cg} is a constant describing the maximum contact guidance effect and k^{cg}_1 and k^{cg}_2 curve fitting parameters determining the transition point and slope of the sigmoid curve.

2.2.2 Collagen fibers

Collagen fiber stress was similarly defined as a summation of anisotropic stress components

$$\boldsymbol{\sigma}_{\mathrm{cf}} = \sum_{i=1}^{N} \phi_{\mathrm{cf}}^{i} \sigma_{\mathrm{cf}}^{i} \boldsymbol{e}_{\mathrm{f}}^{i} \boldsymbol{e}_{\mathrm{f}}^{i} \tag{9}.$$

The total collagen volume fraction remained constant such that

$$\phi_{\mathrm{cf}}^{\mathrm{tot}} = \sum_{i=1}^{N} \phi_{\mathrm{cf}}^{i} \tag{10},$$

with a uniform collagen distribution in-plane ($\phi_{\mathrm{cf}}^{i} = \frac{\phi_{\mathrm{cf}}^{\mathrm{tot}}}{N}$) as starting condition to prevent any directional bias in our results. The collagen fiber stress magnitude σ_{cf}^{i} exhibited a non-linear strain hardening response to tension only

$$\sigma_{\mathrm{cf}}^{i} = \begin{cases} 0 & \text{if } \lambda_{\mathrm{e}}^{i} < 1 \\ k_1 (\lambda_{\mathrm{e}}^{i})^2 (\mathrm{e}^{k_2((\lambda_{\mathrm{e}}^{i})^2 - 1)} - 1) & \text{if } \lambda_{\mathrm{e}}^{i} \geq 1 \end{cases} \tag{11},$$

with k_1 and k_2 material parameters describing the strain hardening response and λ_{e}^{i} the elastic collagen fiber stretch. λ_{e}^{i} can be different from the global stretch λ_{f}^{i} due to the inclusion of collagen prestretch by the fibroblast. Following previous studies (Loerakker et al. 2014; Ristori et al. 2018a), the global stretch was decomposed into an elastic (λ_{e}^{i}) and inelastic (λ_{g}^{i}) component

$$\lambda_{\mathrm{f}}^{i} = \lambda_{\mathrm{e}}^{i} \lambda_{\mathrm{g}}^{i} \tag{12},$$

where λ_{g}^{i} was restricted to ≤ 1 as we only consider collagen crimp. A target value for the inelastic component $\hat{\lambda}_{\mathrm{g}}^{i}$, leading to collagen prestretch, was determined by assuming a mechanical equilibrium between the stress fiber (6) and collagen stress (11) in series (Suppl. A.3). It was assumed that the inelastic component λ_{g}^{i} tends to $\hat{\lambda}_{\mathrm{g}}^{i}$ with a rate characterized by a time constant τ_{λ} via

$$\frac{\mathrm{d}\lambda_{\mathrm{g}}^{i}}{\mathrm{d}t} = \frac{1}{\tau_{\lambda}} (\hat{\lambda}_{\mathrm{g}}^{i} - \lambda_{\mathrm{g}}^{i}) \tag{13}.$$

Collagen (re)orientation was modeled as a redistribution of collagen volume fractions in fiber directions i through direction-dependent degradation and production. Consequently, changes in collagen orientation emerge from preferential collagen turnover rather than from physical rotation of existing collagen fibers. Collagen (re)orientation was modeled as the result of degradation and production in directions i

$$\frac{\mathrm{d}\phi_{\mathrm{cf}}^{i}}{\mathrm{d}t} = f_{\mathrm{prod}}(\varepsilon_{\mathrm{e}}^{i}, \phi_{\mathrm{cf}}^{i}) - \frac{\phi_{\mathrm{cf}}^{i}}{\tau_{\mathrm{cf}}} f_{\mathrm{deg}}(\varepsilon_{\mathrm{e}}^{i}) \tag{14},$$

with τ_{cf} the (re)orientation rate for collagen and $\varepsilon_{\mathrm{e}}^{i} = 0.5((\lambda_{\mathrm{e}}^{i})^2 - 1)$ the directional elastic strain. As discussed by Loerakker et al. (2014), several hypotheses have been proposed regarding mechano-mediated collagen production and degradation mechanisms. We therefore evaluated different scenarios for collagen production and degradation in the cardiac simulations. For the baseline model, we assumed cell-mediated production such that new collagen was produced along the current fibroblast orientation

$$\begin{aligned} &f_{\mathrm{prod}}(\varepsilon_{\mathrm{e}}^{i}, \phi_{\mathrm{sf}}^{i}, \phi_{\mathrm{cf}}^{i}) \\ &= \frac{\phi_{\mathrm{sf}}^{i}}{\sum_{j=1}^{N} \phi_{\mathrm{sf}}^{j}} \sum_{j=1}^{N} \frac{\phi_{\mathrm{cf}}^{j}}{\tau_{\mathrm{cf}}} f_{\mathrm{deg}}(\varepsilon_{\mathrm{e}}^{j}) \end{aligned} \tag{15}.$$

Alternatively, we studied the effect of isotropic collagen production on the (re)orientation of the fibers via

$$f_{\mathrm{prod}}(\varepsilon_{\mathrm{e}}^{i}, \phi_{\mathrm{cf}}^{i}) = \frac{1}{N} \sum_{j=1}^{N} \frac{\phi_{\mathrm{cf}}^{j}}{\tau_{\mathrm{cf}}} f_{\mathrm{deg}}(\varepsilon_{\mathrm{e}}^{j}) \tag{16}.$$

Similarly, two alternative observed patterns for strain-mediated collagen degradation $f_{\mathrm{deg}}(\varepsilon_{\mathrm{e}}^{i})$ were included. The baseline model assumed a V-shaped strain-mediated directional degradation curve with minimized collagen degradation at a transition strain $\varepsilon_{\mathrm{trans}}$ (Gaul et al. 2018; Ghazanfari et al. 2016; Huang and Yannas 1977) (Figure 1c; Suppl. A.4). Alternatively, a monotonically declining curve was assumed, favoring less degradation and thus collagen (re)orientation toward higher strains (Wyatt et al. 2009) (Figure 1c; Suppl. A.4).

2.2.3 Non-fibrous matrix

The stress contribution of the remaining non-fibrous matrix, $\boldsymbol{\sigma}_{\mathrm{m}}$, was modeled with an isotropic,

compressible Neo-Hookean hyperelastic material model

$$\boldsymbol{\sigma}_{\mathrm{m}} = \phi_{\mathrm{m}}\Big(\kappa\frac{\ln(J)}{J}\boldsymbol{I} + \frac{G}{J}\big(\boldsymbol{B} - J^{\frac{2}{3}}\boldsymbol{I}\big)\Big) \quad (17),$$

where ϕ_{m} is the volume fraction of the non-fibrous matrix components, while κ and G are the bulk and shear modulus, respectively. Given the shear modulus G, the bulk modulus was estimated via the following relationship

$$\kappa = \frac{2G(1+\nu)}{3(1-2\nu)} \quad (18),$$

with ν the material's Poisson's ratio. Furthermore, $J = \det(\boldsymbol{F})$ in (17) is the volume ratio, $\boldsymbol{B} = \boldsymbol{F}\cdot\boldsymbol{F}^{\mathrm{T}}$ the left Cauchy-Green strain tensor and $\boldsymbol{I}$ the identity tensor.

2.2.4 Material properties

Material properties of the mechano-mediated tissue (re)orientation model were based on experimental data and previous computational studies (Table 1). The collagen fiber material properties were fitted such that the passive material stress in the tissue (re)orientation model ($\boldsymbol{\sigma}_{\mathrm{tissue}}$ in (2)) corresponded to the passive stress extracted from the healthy left ventricle FE model ($\boldsymbol{\sigma}_{\mathrm{pas}}$ in (1)). Infarct stiffening was represented by an increase in $\phi_{\mathrm{cf}}^{\mathrm{tot}}$. Additionally, the most sensitive parameters causing collagen (re)orientation were calibrated within experimentally constrained ranges using an optimization algorithm to reproduce the physiological transmural collagen organization at the equator.

2.3 Coupling of left ventricular mechanics with collagen (re)orientation model

Spatiotemporal deformations throughout the cardiac cycle were extracted from the left ventricle FE model as components of the deformation gradient tensor $\boldsymbol{F}$ (Figure 1b). The deformation gradient components were determined in a local, right-handed cardiac coordinate system ($\boldsymbol{e}_{\mathrm{c}}$, $\boldsymbol{e}_{\mathrm{l}}$, $\boldsymbol{e}_{\mathrm{t}}$) corresponding to the circumferential, longitudinal, and transmural directions. Subsequently, these local deformations were imposed as displacement boundary conditions in a linear hexahedral element with reduced integration (C3D8R) in Abaqus Standard (Dassault Systèmes Simulia Corp. 2024) via

$$\boldsymbol{u} = (\boldsymbol{F} - \boldsymbol{I})\boldsymbol{x}_0 \quad (19).$$

The mechano-mediated collagen (re)orientation model described previously was coded for this single element model via a user-defined material subroutine (UMAT). Collagen (re)orientation was modeled in the $(\boldsymbol{e}_{\mathrm{c}}, \boldsymbol{e}_{\mathrm{l}})$-plane, with the resulting distribution characterized by a helix angle α_{h} (see (23) and Figure 1c). Using this approach, we implicitly incorporated cardiomyocyte contraction from the left ventricle model as a stimulus for mechano-mediated reorientation of the non-cardiomyocyte components of the left ventricle (Mostert et al. 2022; Simpson et al. 1994).

2.4 Numerical approximation

Solving the ordinary differential equations (ODEs) in (7), (13), and (14) through direct time integration is computationally infeasible due to the large separation in timescales between cardiac strains calculated by the FE model, which vary over seconds, and mechano-mediated (re)orientation of the collagen fibers, which occurs over weeks. For this reason, we adopted a previously established approximation algorithm to efficiently solve these ODEs (Ristori et al. 2016). Briefly, it was found that the periodic solutions of these ODEs with dynamic strain input converge to an almost constant asymptotic solution for $t \to \infty$. These asymptotic solutions, hereafter referred to as preferred solutions following Ristori et al. (2016), are denoted by ($\phi^i_{\mathrm{sf,P}}$, $\phi^i_{\mathrm{cf,P}}$ and $\hat{\lambda}^i_{\mathrm{g,P}}$). They were obtained by numerically integrating the evolution laws. For more details on the numerical integration procedure, we refer to Ristori et al. (2016) and Supplementary A.5. The temporal evolution of ϕ^i_{sf}, ϕ^i_{cf} and λ^i_{g} toward their preferred steady-state solutions was modeled using a first-order linear rate equation solved with implicit Euler numerical integration

$$\frac{\mathrm{d}\phi^i_{\mathrm{sf}}}{\mathrm{d}t} = \frac{1}{\tau_{\mathrm{sf}}}(\phi^i_{\mathrm{sf,P}} - \phi^i_{\mathrm{sf}}) \quad (20),$$

Table 1 Parameters of the mechano-mediated collagen (re)orientation model

Constituent	Model Parameter	Value	References
Stress Fibers	$\sigma_{\max}$ [kPa]	1.5	(Deshpande et al. 2006; Hermans 2024; Yang et al. 2021)
	ε_0 [-]	0.11	(McEvoy et al. 2019; Obbink-Huizer et al. 2014; Vernerey and Farsad 2011)
	ε_1 [-]	0.28	(McEvoy et al. 2019; Obbink-Huizer et al. 2014; Vernerey and Farsad 2011; Vigliotti et al. 2016)
	k_{v} [s]	50	(Obbink-Huizer et al. 2014)
	$\phi_{\mathrm{sf}}^{\mathrm{tot}}$ [-]	0.05	(Obbink-Huizer et al. 2014)
	k_0^{f} [s^{-1}]	1.7×10^{-6}	(Obbink-Huizer et al. 2014)
	k_1^{f} [$\mathrm{s}^{-1} \cdot \mathrm{MPa}^{-1}$]	0.37	(Obbink-Huizer et al. 2014; Vernerey and Farsad 2011)
	k_{d} [s^{-1}]	1.3×10^{-3}	(Obbink-Huizer et al. 2014)
	g_{cg} [s^{-1}]	2.8	(Ristori et al. 2018b)
	k_1^{cg} [-]	142	(Ristori et al. 2018b)
	k_2^{cg} [-]	214	(Ristori et al. 2018b)
	τ_{sf} [s]	230	(van Vlimmeren et al. 2012)
Collagen	k_1 [kPa]	0.94	fitted (Bovendeerd et al. 2009)
	k_2 [-]	4.0	fitted (Bovendeerd et al. 2009)
	$\phi_{\mathrm{cf}}^{\mathrm{tot}}$ Healthy [-]	0.33	(Greiner et al. 2018; Pope et al. 2008)
	$\phi_{\mathrm{cf}}^{\mathrm{tot}}$ Infarct [-]	0.7	(Greiner et al. 2018; Guan et al. 2025; Pope et al. 2008)
	$D_{\max}$ [-]	1.0	(Loerakker et al. 2013)
	$D_{\min}$ [-]	0.059	(Ghazanfari et al. 2016; Yeganegi et al. 2023)
	D_{40} [-]	0.52	(Ghazanfari et al. 2016)
	$\varepsilon_{\mathrm{trans}}$ [-]	0.18	(Ghazanfari et al. 2016; Yeganegi et al. 2023)
	τ_λ [h]	1	(Visser et al. 2025)
	τ_{cf} [h]	12	(Visser et al. 2025)
Matrix	G Healthy [MPa]	0.03	fitted (Bovendeerd et al. 2009)
	G Infarct [MPa]	0.10	fitted (Janssens et al. 2023)
	Poisson's ratio ν [-]	0.47	(Bovendeerd et al. 2009)

$$\frac{\mathrm{d}\phi_{\mathrm{cf}}^i}{\mathrm{d}t} = \frac{1}{\tau_{\mathrm{cf}}}(\phi_{\mathrm{cf,P}}^i - \phi_{\mathrm{cf}}^i) \quad (21),$$

$$\frac{\mathrm{d}\lambda_{\mathrm{g}}^i}{\mathrm{d}t} = \frac{1}{\tau_\lambda}(\hat{\lambda}_{\mathrm{g,P}}^i - \lambda_{\mathrm{g}}^i) \quad (22).$$

2.5 Postprocessing

The main outcome of our study is a vector of in-plane collagen volume fractions $\tilde{\boldsymbol{\phi}}_{\mathrm{cf}} = [\phi_{\mathrm{cf}}^1, \phi_{\mathrm{cf}}^2, \ldots, \phi_{\mathrm{cf}}^N]^{\mathrm{T}}$. These results were subsequently normalized such that $\bar{\phi}_{\mathrm{cf}}^i = \phi_{\mathrm{cf}}^i / \max(\tilde{\boldsymbol{\phi}}_{\mathrm{cf}})$, and circular statistics were applied. In particular, the mean collagen fiber orientation (helix angle α_{h}) was calculated by

$$\alpha_{\mathrm{h}} = \frac{90}{\pi}\,\mathrm{atan2}\left(\sum_{i=1}^{N} \bar{\phi}_{\mathrm{cf}}^i \sin(2\gamma^i), \sum_{i=1}^{N} \bar{\phi}_{\mathrm{cf}}^i \cos(2\gamma^i)\right) \quad (23),$$

where doubling the angle ($2\gamma^i$) accommodates the axial symmetry of the fibers. Additionally, an anisotropy index S was calculated based on

circular statistics

$$S = \frac{\sqrt{\left(\sum_{i=1}^{N} \bar{\phi}_{\mathrm{cf}}^{i} \cos(2\gamma^{i})\right)^{2} + \left(\sum_{i=1}^{N} \bar{\phi}_{\mathrm{cf}}^{i} \sin(2\gamma^{i})\right)^{2}}}{\sum_{i=1}^{N} \bar{\phi}_{\mathrm{cf}}^{i}} \quad (24),$$

where $S = 0$ describes an isotropic distribution of collagen fibers, and $S = 1$ a completely anisotropic distribution. Postprocessing was performed in MATLAB R2023a (The MathWorks Inc. 2023) using the Abaqus2Matlab toolbox (Papazafeiropoulos et al. 2017).

3 Results

3.1 Mechanobiological mechanisms of collagen organization can replicate physiological left ventricular alignment

We first investigated collagen (re)orientation at the equator for four transmural locations (20%, 40%, 60% and 80% along the endo- to epicardium wall trajectory; Figure 2a) using our mechanobiology-informed computational framework. An optimization algorithm was used to identify parameter values for stress fiber contraction ($\sigma_{\max}$), minimized strain-mediated collagen degradation ($\varepsilon_{\mathrm{trans}}$), and contact guidance (k_1^{cg}, k_2^{cg}, g_{cg}) that produced physiological collagen orientations, with all parameters constrained to ranges reported in the literature during the optimization. The resulting steady-state collagen orientations were characterized by a transmural transition from right-handed helical fibers near the endocardium ($+\alpha_{\mathrm{h}}$) to left-handed helical fibers near the epicardium ($-\alpha_{\mathrm{h}}$) (Figure 2b). Moreover, collagen volume fractions revealed a strong unidirectional alignment at all transmural locations (Figure 2c; average anisotropy index $S = 0.97$ [-]). Notably, this mechanobiology-driven transmural transition in helix angle largely corresponds to the reference alignment used in the finite element model ($R^2 = 0.73$) (Figure 2b). Repeating the same analysis at two additional locations along the base-to-apex trajectory resulted in similar transmural collagen fiber orientations (Figure 2b, e, g). This consistency in base-to-apex transmural trajectories is in agreement with *in vivo* measurements (Walker et al. 2005) (Suppl. Figure 7).

3.2 Left ventricular collagen orientation corresponds to strain with minimized degradation

The local dynamic strain environment, in combination with the inclusion of a V-shaped, strain-mediated collagen degradation law in the model, provides an explanation for the collagen fiber orientations in Figure 2b. Since local strain profiles are similar transmurally for the different base-to-apex locations (Figure 2d, f, h), we focus on explaining strain-mediated collagen orientation patterns along the endo- to epicardial direction. During the peak-diastolic phase, circumferential strains near the endocardium (20% wall distance; $\varepsilon_{\mathrm{cc}} \approx 0.39$ [-]) are well above the transition strain $\varepsilon_{\mathrm{trans}} = 0.18$ [-] of the V-shaped curve, associated with relatively high degradation rates in the circumferential direction. In contrast, peak-diastolic longitudinal strains near the endocardium ($\varepsilon_{\mathrm{ll}} \approx 0.19$ [-]) are closer to the optimum $\varepsilon_{\mathrm{trans}}$, coinciding with relatively low degradation rates. As a result, collagen fibers near the endocardium align toward the longitudinal direction. Moving away from the endocardium, both peak-diastolic circumferential and longitudinal strains gradually decrease to equal values near the epicardium (80% wall distance; $\varepsilon_{\mathrm{cc}} \approx 0.14$ [-] and $\varepsilon_{\mathrm{ll}} \approx 0.13$ [-]). The transmural decrease in circumferential strain, approaching the optimum value $\varepsilon_{\mathrm{trans}}$, reduces the degradation rate in that direction. In contrast, decreasing longitudinal strains lead to an increasing degradation rate. Together, these local, strain-dependent collagen degradation dynamics initiate the transmural transition in fiber orientation, with fibers becoming increasingly circumferentially aligned toward the epicardium.

While we previously demonstrated that nominal strains dictate the primary endocardium to epicardium transition from more longitudinal to more circumferential collagen fiber orientations, shear strains are crucial for establishing the characteristic transmural helix-angle profile. Although modest in magnitude during the cardiac cycle (peak value of $\varepsilon_{\mathrm{cl}} \approx -0.05$ [-]; Figure 2d, f, h), shear strain can, in combination with the nominal loading, adjust the direction that satisfies the optimized strain $\varepsilon_{\mathrm{trans}}$ associated with the minimum collagen degradation. For instance, near the endocardium (20%) and at mid-wall (40% and 60% wall distance), circumferential strain components that

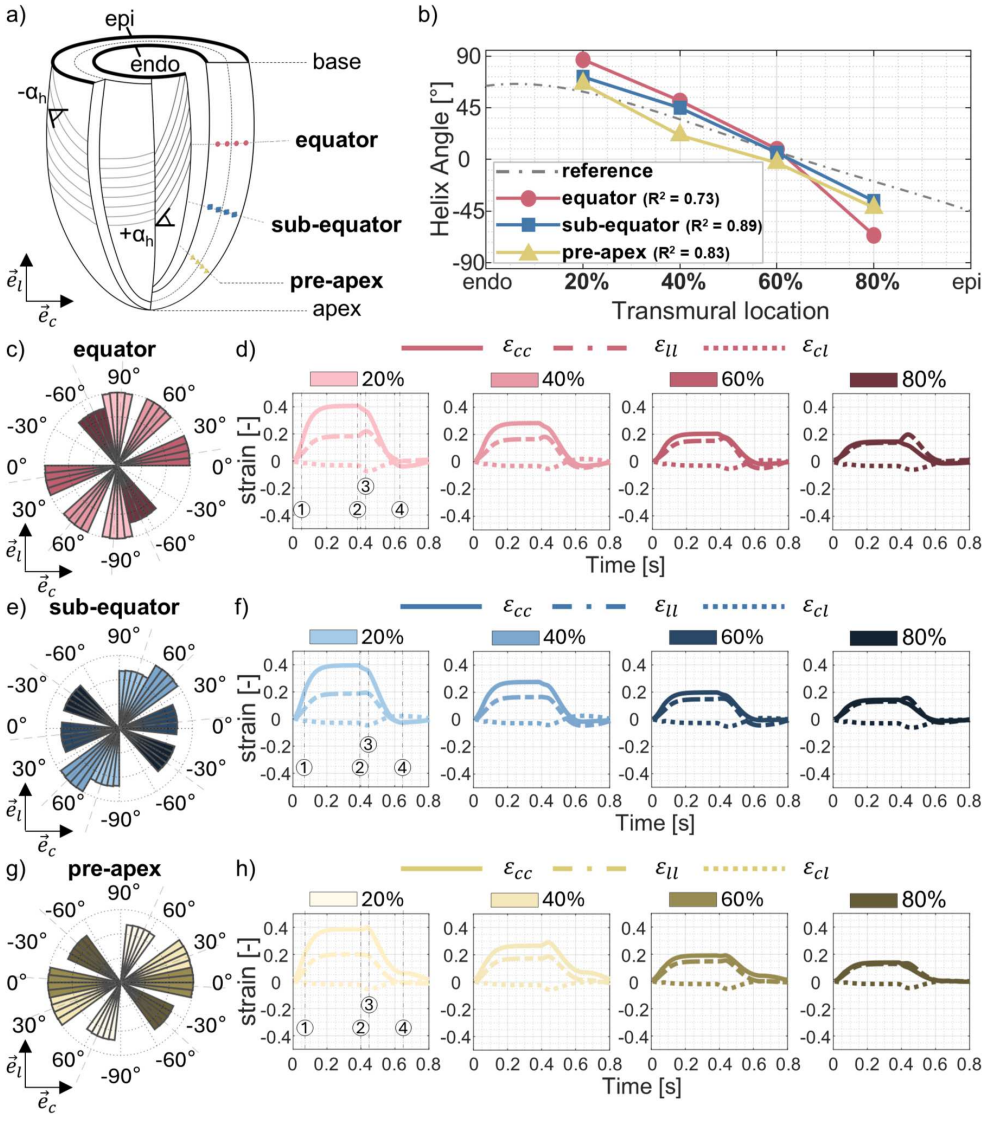


Fig. 2 Computational results for mechano-mediated collagen fiber (re)orientation in the healthy left ventricle. a) Left ventricular FE model, displaying the double-helical structure in the circumferential-longitudinal plane ($\boldsymbol{e}_c, \boldsymbol{e}_l$-plane). Extracted locations for tissue remodeling are located at the equator and 35% and 65% below the equator. b) Resulting mean collagen fiber helix angle along the transmural trajectory from the (re)orientation model compared with the FE model reference. c), e), g) Transmural collagen volume fraction distributions in-plane, and d), f), h) Green-Lagrange strains for the simulated locations. Numbers indicate the start of the (1) diastolic, (2) isovolumetric contraction, (3) systolic, and (4) isovolumetric relaxation phases

initially exceeded $\varepsilon_{\text{trans}}$ are reduced toward $\varepsilon_{\text{trans}}$ along right-handed helical fiber directions ($+\alpha_{\text{h}}$) because the opposing negative shear strain partially counteracts the circumferential strain. This strain adjustment amplifies the transition from longitudinal to circumferential collagen alignment which is already driven by the nominal strains. Strikingly, near the epicardium (80% wall distance), shear strain becomes the dominant factor in maintaining a left-handed collagen orientation ($-\alpha_{\text{h}}$). In this location, equal nominal strains below the optimum $\varepsilon_{\text{trans}}$ provide no preferred direction that would minimize collagen degradation. Under these conditions, the presence of negative shear strain increases the strain of collagen fibers aligned with the shear direction toward $\varepsilon_{\text{trans}}$, thereby promoting a left-handed helical alignment. Overall, the physiological transmural transition from right-handed fibers near the endocardium to left-handed fibers near the epicardium can only be reproduced when shear strain is included alongside the circumferential and longitudinal strain.

3.3 Variations in strain-dependent collagen degradation result in non-physiological cardiac collagen organization

To investigate the role of strain-mediated collagen degradation in cardiac collagen organization, we altered strain-mediated collagen degradation characteristics. We found that decreasing (0.5x) or increasing (1.5x) the optimum strain value $\varepsilon_{\text{trans}}$ in the V-shaped degradation curve failed to reproduce the characteristic transition in helical alignment, resulting in either a transmurally uniform right-handed or left-handed helical organization instead (Figure 3a). Furthermore, a monotonic relation of collagen degradation with strain failed to capture a transmural transition in helical alignment for equal or increased values of $\varepsilon_{\text{trans}}$ (Figure 3b). Although a monotonic degradation curve with a lower $\varepsilon_{\text{trans}}$ appears to result in a qualitatively similar endo- to epicardium transition in collagen orientations, inspection of the 20% wall location together with additional simulations revealed deviations from the physiological transmural helix-angle profile (Suppl. Figure 11). Specifically, the monotonic degradation curve consistently predicted more left-handed, epicardial-like collagen orientations in the subendocardial region. These findings suggest that physiological collagen organization in the left ventricle requires a directionally regulated strain-dependent degradation mechanism in which degradation increases at both low and high strain magnitudes and is minimized at an intermediate strain.

3.4 Left ventricular collagen orientation requires fibroblast-collagen interplay

To assess whether mechanisms other than strain-mediated collagen degradation contribute to physiological cardiac collagen organization, we varied model components describing fibroblast-mediated effects on collagen reorientation. We examined the importance of directional collagen deposition by the fibroblasts on cardiac collagen organization by exploring two mechanistic variations: loss of contact guidance with the collagen while maintaining collagen synthesis along the cytoskeletal axis, and the use of isotropic collagen synthesis while maintaining contact guidance. The first case resulted in unphysiological, transmurally uniform right-handed collagen orientations (Figure 4a). In the absence of contact guidance, fibroblasts orient along the direction of minimal strain (strain avoidance), resulting in misaligned collagen deposition in transmural locations close to the epicardium. In the alternative case of isotropic collagen production, native-like collagen alignment was preserved but accompanied by a substantial loss in tissue anisotropy, to the extent that no clear dominant collagen orientation remained (Figure 4b). Together, these findings suggest that physiological unidirectional collagen alignment in the left ventricle requires both contact guidance and directional fibroblast-mediated collagen synthesis as losing either mechanism leads to unphysiological collagen alignment, reduced anisotropy, or both.

We next varied the magnitude of maximum fibroblast contraction σ_{max}, based on earlier work demonstrating the critical role of this parameter in the prediction of collagen orientation in paediatric heart valves (Ristori et al. 2018a). Increasing σ_{max} resulted in predominantly right-handed helical fibers, whereas decreasing σ_{max} maintained native-like collagen orientations (Figure 5). These

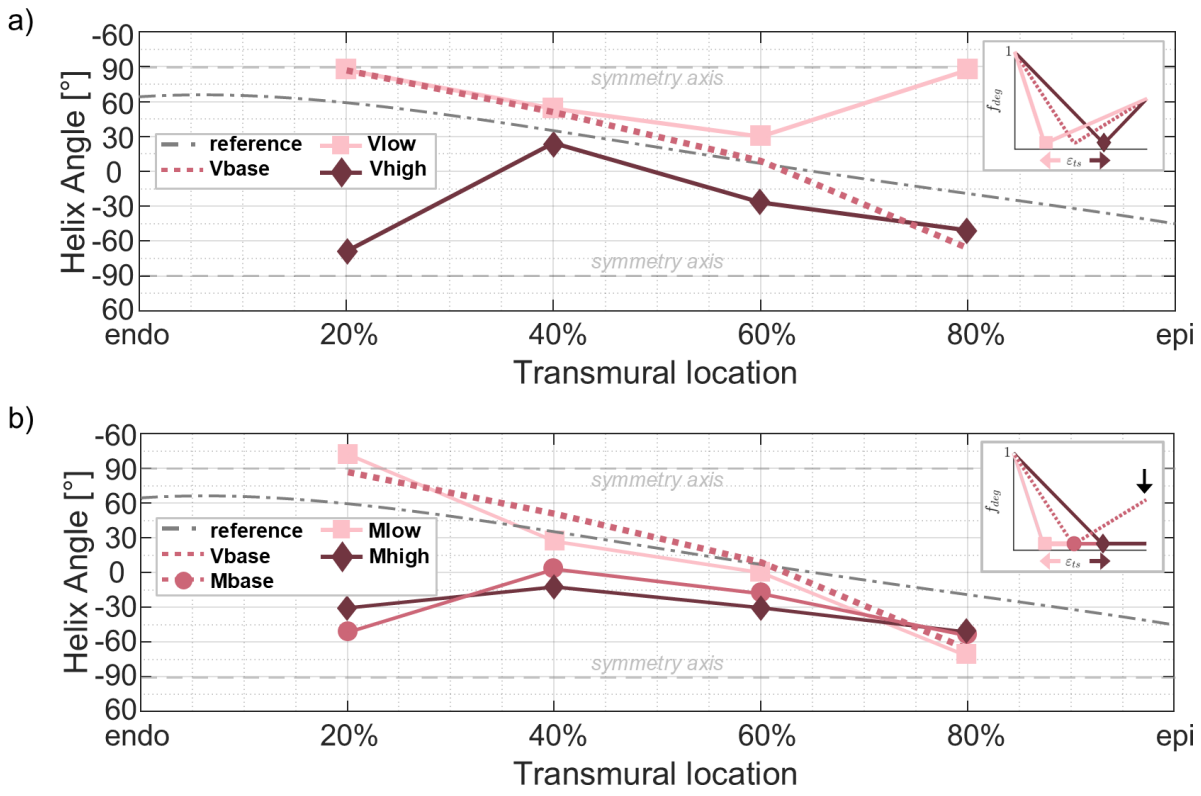


Fig. 3 Effect of variations in the strain-mediated collagen degradation curve on predicted mean collagen helix angles at the equator. a) 50% left (V_{low}) and right (V_{high}) shift of the transition strain in the V-shaped curve. A value of $\varepsilon_{trans} = 0.18$ is used for the baseline model (V_{base}). Results are compared with the FE model reference. b) Monotonic degradation curve applied with either the same ε_{trans} as in the optimized V-shaped curve (M_{base}) or 50% left (M_{low}) and right (M_{high}) shift in ε_{trans}. The symmetry axes in both plots are included to account for axial symmetry in collagen fiber orientations

results indicate that fibroblast-mediated collagen reorientation is limited under physiological conditions in the left ventricle. Elevated fibroblast contractility may promote cell reorientation independent from the collagen orientation through strain avoidance, leading to collagen deposition that is misaligned with the existing collagen network. In addition, increased collagen prestretch may alter the strain-mediated degradation cues that determine the collagen orientation as shown previously. These simulations therefore suggest that both mechanisms are constrained under physiological conditions.

3.5 Altered tissue strains in infarction drive strain-dependent collagen reorientation

Lastly, we applied our computational framework to simulate an infarcted heart and assessed whether pathological collagen fiber orientation can be explained by the same mechanobiological mechanisms that lead to physiological collagen orientation. Here, we observed that the altered mechanical environment within the infarcted region resulted in a predominantly circumferential collagen fiber organization for most transmural locations (Figure 6). This organization deviates from the transmurally varying fiber orientation implemented in the finite element model, yet is consistent with structural observations from *ex vivo* large animal LAD infarction models reporting circumferentially biased fiber orientations within the

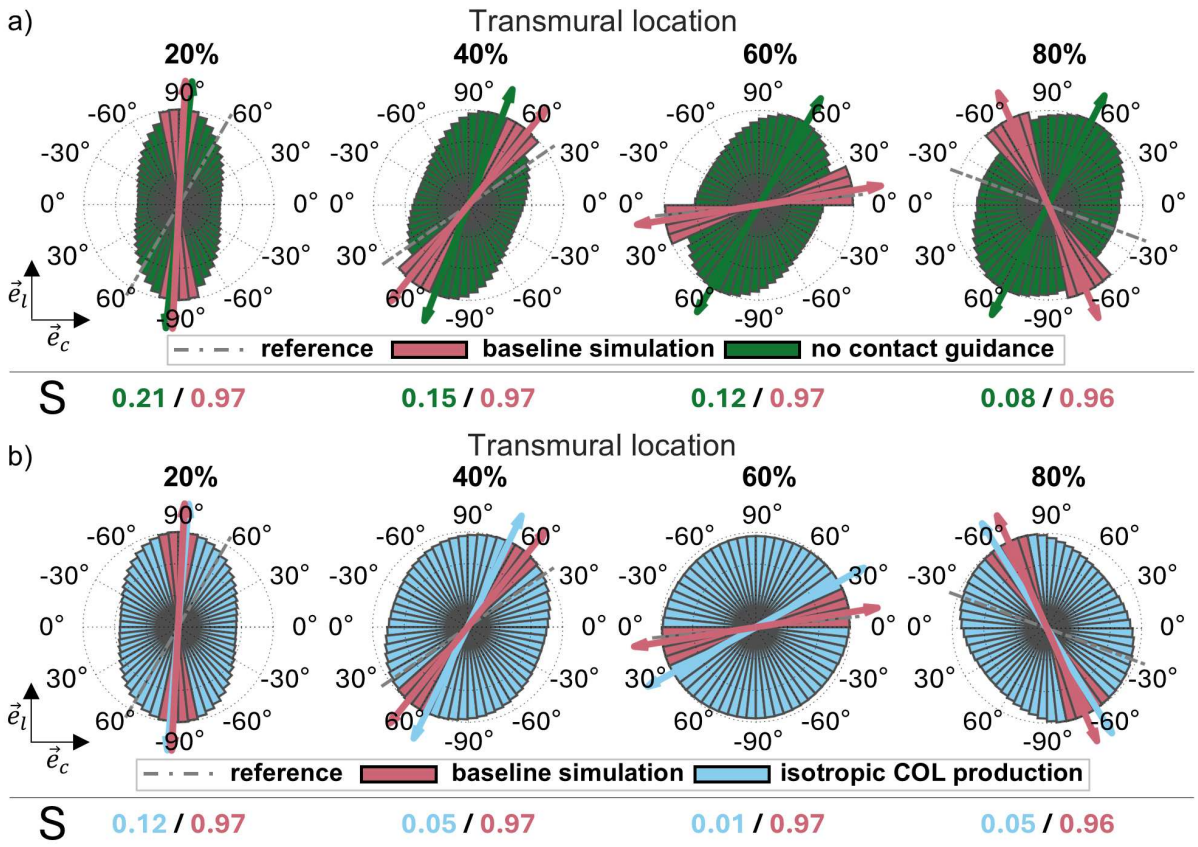


Fig. 4 Resulting collagen volume fractions on the equator after a) exclusion of the contact guidance cue and b) imposing isotropic collagen synthesis by fibroblasts. The colored arrows show the mean collagen orientation while the dash-dotted line is the FE model reference orientation. Additionally, the anisotropy index S [0 - isotropic, 1 - fully anisotropic] is given for each simulation

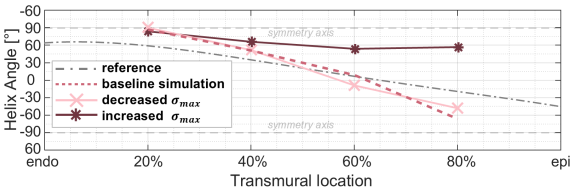


Fig. 5 Variations in fibroblast contractility ($\sigma_{\max}$) on transmural collagen orientation in the left ventricle. $\sigma_{\max}$ was respectively decreased to a value of 0.15 [kPa] or increased to 15.0 [kPa]

infarcted myocardium (Gupta et al. 1994; Hervas et al. 2016; Wu et al. 2006).

Furthermore, in contrast to highly aligned collagen fibers in the healthy myocardium, a larger dispersion in collagen fiber orientations and therefore lower structural anisotropy is observed for the infarcted region (Figure 6b). Quantitatively, this corresponds to an average decrease of 43% in anisotropy index S compared to simulations in healthy myocardium, which is similar to the decrease in fractional anisotropy (FA) measured in *ex vivo* porcine models of LAD infarction (Wu et al. 2006). In the computational model, this loss in anisotropy can be attributed to the higher collagen content in the infarct ($\phi_{\text{cf}}^{\text{tot}} = 0.7$ [-]) which reduces the directional sensitivity of the contact-guidance cue due to saturation at higher directional collagen volume fractions. As a result, the predicted anisotropy becomes weaker. Removing the contact guidance cue entirely, however, yields an increased transmural longitudinal collagen fiber alignment that is not observed experimentally (Figure 6d). These results therefore indicate that the collagen fiber organization observed in the infarcted region may arise through (some degree of) structural guidance of fibroblasts combined with collagen synthesis along the fibroblast's

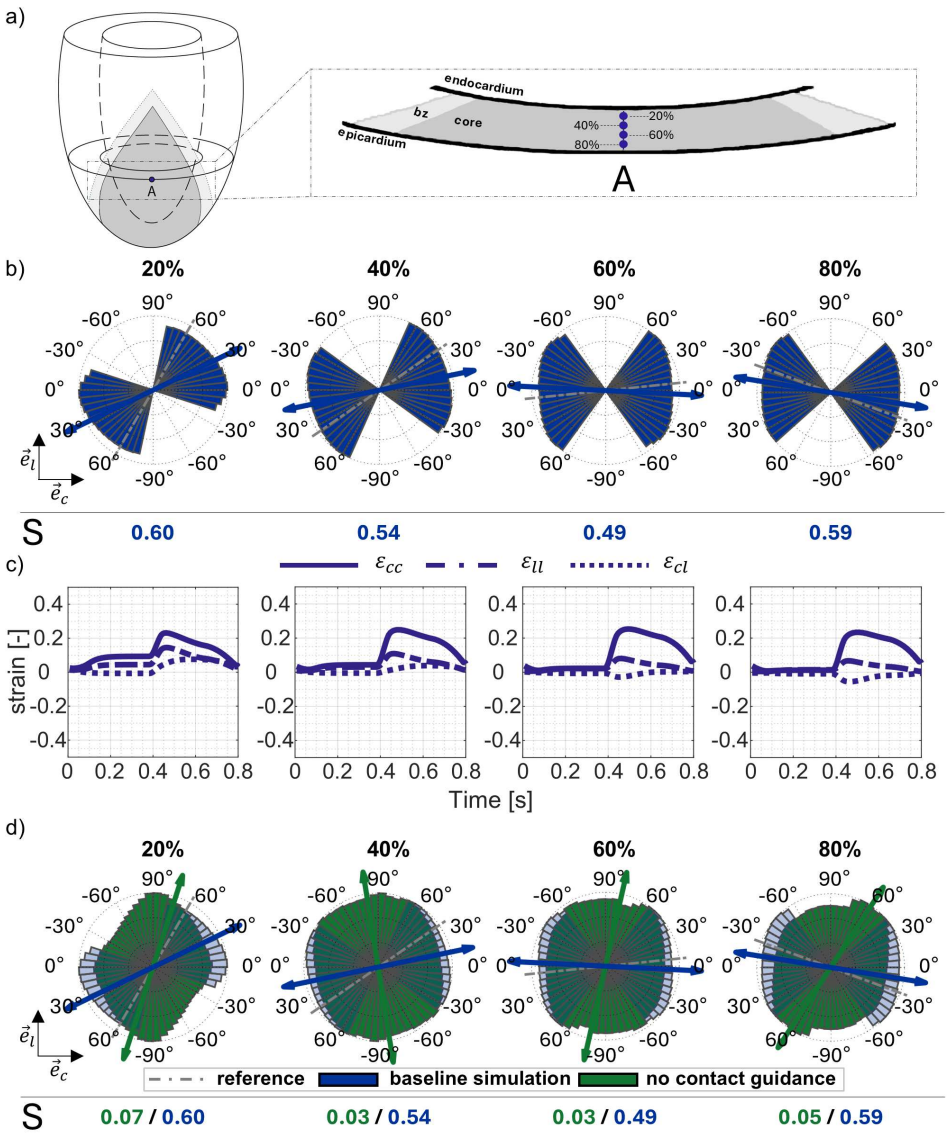


Fig. 6 Collagen (re)orientation in a model of LAD occlusion myocardial infarction. a) FE model of the LAD infarct representing the infarcted (gray) and border zone (light-gray) regions. b) Transmural collagen volume fractions in the infarct core. The arrows depict the main collagen fiber orientation. Additionally, the anisotropy index S [0-1] is given for each simulation. c) Green-Lagrange strains for the transmural wall locations in the infarct core. d) Resulting collagen volume fractions in the infarct core with and without inclusion of the contact guidance cue

cytoskeletal axis, analogous to the situation in the healthy myocardium.

4 Discussion

The mechanobiological mechanisms regulating collagen fiber orientation in the left ventricle remain incompletely understood despite their importance in maintaining cardiac structural homeostasis. A deeper understanding of these mechanisms could inform novel targeted strategies to control or even reverse adverse structural remodeling in cardiac pathologies. To investigate the mechanobiological determinants of cardiac collagen orientation, we developed a multiscale computational framework that couples left ventricular strains to experimentally informed mechanisms of collagen reorientation. The resulting simulations reproduced the physiological collagen fiber organization of the healthy adult left ventricle (Figure 2), suggesting that currently known mechanisms of mechano-mediated collagen reorientation may contribute substantially to the regulation of cardiac collagen architecture. Furthermore, the framework provides a platform to examine the relative roles of the individual mechanisms involved in this process.

Our results specifically indicate that a non-monotonic, V-shaped relation between strain and directionally dependent collagen degradation is necessary to preserve the physiological left ventricular collagen organization (Figure 3a,b). This suggests that, if strain-dependent collagen degradation contributes to left ventricular structural homeostasis, it is unlikely to be governed by a purely strain-stabilizing monotonic response. It is well established that myocardial collagen fibers are not aligned with the maximum principal strain direction, but are instead organized to promote a homogeneous distribution of fiber strain across the left ventricular wall (Carruth et al. 2016; Mehri et al. 2024; Moulin et al. 2021; Wang et al. 2016). This observation is difficult to interpret with a monotonic strain-degradation relation, which would favor collagen orientation in the dominant strain direction. Instead, it is consistent with selective degradation of both unloaded and excessively strained fibers, as represented by the V-shaped curve. Combined with recent observations of similar V-shaped degradation patterns in other collagenous tissue types (Barbour and Huang 2020; Deng et al. 2024; Gaul et al. 2018; Jenkins et al. 2026; Richardson et al. 2018; Yi et al. 2016), our results provide a testable hypothesis for future experimental studies on strain-dependent collagen degradation in myocardial tissue.

Our simulations further indicate that cardiac fibroblasts embedded within the physiological left ventricular collagen matrix primarily contribute to the maintenance of established collagen alignment rather than driving the network's orientation. We showed that the physiological collagen organization strongly depends on a synergistic interaction between fibroblast-mediated collagen deposition along the cellular axis and contact guidance cues that maintain fibroblast alignment with the collagen fibers (Figure 4). By comparison, model variations that increased the ability of fibroblasts to dictate collagen orientation produced non-physiological collagen architectures (Figure 5). These findings are consistent with experimental observations that cardiac fibroblasts adopt a quiescent phenotype in aligned environments with physiological cardiac stiffness (Atance et al. 2004; Pereira-Sousa et al. 2026; Pesce et al. 2023; Shinde et al. 2017). Our simulations provide a potential mechanistic link between this quiescent fibroblast phenotype and physiological collagen alignment in the left ventricle, suggesting that elevation of fibroblast contractility alone may be sufficient to compromise this collagen architecture, even in the absence of altered strain fields.

Another notable finding is that, in an infarcted left ventricle, the same mechanobiological mechanisms that maintain physiological collagen organization no longer favor the native double-helical architecture, but instead give rise to collagen fiber orientations and disarray consistent with experimental observations in infarcts (Figure 6) (Gupta et al. 1994; Hervas et al. 2016; Wu et al. 2006). Although similar mechanobiological mechanisms have previously been shown to contribute to infarct collagen restructuring (Fomovsky et al. 2012; Richardson and Holmes 2016), the present work suggests that infarct collagen reorientation and maintenance of physiological cardiac collagen organization may be governed by the same underlying mechanisms. This raises the possibility that pathological collagen reorientation may be understood, at least in part, as the response of physiological maintenance mechanisms to an altered

mechanical environment, providing a mechanistic basis for future studies aimed at evaluating how therapeutic alterations of the mechanical environment of the heart may influence cardiac tissue organization.

One limitation in our study is that the material model of the left ventricle was not updated based on the predicted collagen orientations. Changes in structural alignment can alter ventricular deformation patterns (Barbarotta and Bovendeerd 2021), which may in turn influence the mechano-mediated collagen (re)orientation. Consequently, the present model should be interpreted as a method to understand the mechanobiological mechanisms responsible for the maintenance of collagen organization in physiological and pathological conditions rather than a model of temporal cardiac remodeling. Future studies could address this limitation through a two-way coupled framework in which collagen (re)orientation and left ventricular mechanics are both updated over time.

A second limitation is that we implemented the role of cardiomyocytes only via their direct effect on the mechanical environment in the left ventricle, without allowing them to actively participate in mechano-mediated (re)orientation. This choice is supported by the literature (Mostert et al. 2022; Simpson et al. 1994). Nevertheless, other work proposes that the cardiomyocytes themselves can reorient in response to mechanical stimuli by reorganization of their sarcomeric structure (Arts et al. 1994; Williams et al. 2025). While the present study focuses on matrix- and fibroblast-mediated mechanisms of collagen (re)orientation, we acknowledge the possibility that cardiomyocytes, especially in a less mature phenotype, may also contribute to the maintenance of the cardiac collagen network and overall left ventricular structural organization (Mostert et al. 2026).

To conclude, we used computational modeling to reveal that V-shaped strain-mediated directional collagen degradation is a potentially crucial mechanobiological mechanism for the maintenance of left ventricular collagen organization, while embedded cardiac fibroblasts primarily serve a stabilizing rather than a restructuring role. Interestingly, the same mechanobiological mechanisms that maintain physiological collagen organization can promote collagen reorientation under infarct loading conditions, linking physiological structural maintenance to pathological tissue reorganization. These identified mechanisms may help guide future efforts to understand and direct cardiac collagen organization in both regenerative therapies and tissue-engineered cardiac constructs, thereby promoting structurally favorable remodeling following myocardial injury (Kluge et al. 2010; Mostert et al. 2025; Uiterwijk et al. 2020; Weinberger et al. 2016).

Statements and Declarations

Funding. This work was funded by the European Research Council (ERC) under the RE-ALIGN Advanced Grant (grant agreement number 101054726) awarded to C.V.C. Bouten, and by the Gravitation Program "Materials Driven Regeneration", funded by the Netherlands Organization for Scientific Research (NWO; grant number 024.003.013). This work was further supported by the partners of Regenerative Medicine Crossing Borders (https://www.regmedxb.com), powered by Health˜Holland, Top Sector Life Sciences & Health.

Competing interests. The authors have no relevant financial or non-financial interests to disclose.

Ethics approval. Not applicable. This study is purely computational and did not involve human participants or animals; all experimental data used for comparison were obtained from previously published studies.

Data availability. All data will be available at 4TU.ResearchData, through: https://doi.org/10.4121/5475b758-1de6-4547-90bb-e9e50e6a61ea

Code availability. All computational code will be available at 4TU.ResearchData, through: https://doi.org/10.4121/5475b758-1de6-4547-90bb-e9e50e6a61ea

Author contributions. Conceptualization: L.S., H.H., C.B., S.L.; Methodology: L.S., H.H., K.J., T.R., S.L.; Software: L.S., H.H., K.J.; Validation: L.S., H.H.; Formal analysis: L.S., H.H.; Investigation: L.S., H.H.; Data curation: L.S.; Visualization: L.S., H.H.; Writing – original draft: L.S., H.H.; Writing – review & editing: L.S., H.H., K.J., T.R., P.B., C.B., S.L.; Resources:

H.H., K.J., T.R., P.B., C.B., S.L.; Supervision: T.R., P.B., C.B., S.L.; Funding acquisition: C.B. All authors read and approved the manuscript.

Supplementary A Methodology

A.1 Fiber orientation field in left ventricle FE model

The anisotropic material behavior of the left ventricular FE model was governed by a rule-based myofiber architecture adopted from Bovendeerd et al. (2009). The local orientation of the myofibers was described by a helix angle ($\alpha_{\mathrm{h}}^{\mathrm{ref}}$) and a transverse angle ($\alpha_{\mathrm{t}}^{\mathrm{ref}}$). The helix angle $\alpha_{\mathrm{h}}^{\mathrm{ref}}$ defines the orientation of the myofibers within the circumferential-longitudinal plane and is measured relative to the local circumferential direction. Positive and negative values correspond to right-handed and left-handed helical orientations, respectively. The transverse angle $\alpha_{\mathrm{t}}^{\mathrm{ref}}$ describes the deviation of the myofibers out of the circumferential-longitudinal plane toward the transmural direction.

The rule-based method used normalized local coordinates (u, v) to describe the spatial distributions of $\alpha_{\mathrm{h}}^{\mathrm{ref}}$ and $\alpha_{\mathrm{t}}^{\mathrm{ref}}$. The normalized longitudinal coordinate (u) describes the location along the base-to-apex trajectory. Its value varies from $u = +0.5$ at the base, $u = 0$ at the equator and $u = -1$ at the apex. The transmural normalized coordinate v varies linearly along the endo- to epicardium trajectory, specifically from $v = -1$ at the endocardial surface to $v = +1$ at the epicardial surface. The fiber angles are described by

$$\begin{aligned}\alpha_{\mathrm{h}}^{\mathrm{ref}}(u,v) = \\ &\big(h_{10}L_0(v) + h_{11}L_1(v) + h_{12}L_2(v) \\ &+ h_{13}L_3(v) + h_{14}L_4(v)\big) \\ &\cdot \big(1 + h_{22}L_2(u) + h_{24}L_4(u)\big)\end{aligned} \tag{A1}$$

$$\begin{aligned}\alpha_{\mathrm{t}}^{\mathrm{ref}}(u,v) = \\ &\big(1 - v^2\big)\left(1 + t_{11}L_1(v) + t_{12}L_2(v)\right) \\ &\cdot \left(t_{21}L_1(u) + t_{23}L_3(u) + t_{25}L_5(u)\right)\end{aligned} \tag{A2}$$

where $L_k(u)$ and $L_k(v)$ are normalized Legendre polynomials of the kth order. The values for the coefficients are summarized in Table 2.

Table 2 Coefficients describing fiber field in FE model

Coefficient	Value
h_{10}	0.362 [rad]
h_{11}	−1.16 [rad]
h_{12}	−0.124 [rad]
h_{13}	0.129 [rad]
h_{14}	−0.0614 [rad]
h_{22}	0.0984 [-]
h_{24}	−0.0501 [-]
t_{11}	−0.626 [-]
t_{12}	0.502 [-]
t_{21}	0.626 [rad]
t_{23}	0.211 [rad]
t_{25}	0.038 [rad]

A.2 Strain and strain-rate dependent relation to stress fiber stress in cardiac fibroblasts

We modeled the cardiac fibroblast stress contribution as a combination of passive and active contractile stresses. The strain dependent response was subsequently separated into a nonlinear passive strain hardening response ($f_{\varepsilon,\mathrm{p}}$) and a length-tension relationship for actin-myosin sliding leading to active contraction ($f_{\varepsilon,\mathrm{a}}$)

$$f_{\varepsilon} = f_{\varepsilon,\mathrm{p}} + f_{\varepsilon,\mathrm{a}} \tag{A3}$$

$$f_{\varepsilon,\mathrm{p}}(\varepsilon^i) = \begin{cases} 0 & \text{if } \varepsilon^i < 0, \\ \left(\frac{\varepsilon^i}{\varepsilon_1}\right)^2 & \text{if } \varepsilon^i \geq 0. \end{cases} \tag{A4}$$

$$f_{\varepsilon,\mathrm{a}}(\varepsilon^i) = \mathrm{e}^{-\left(\frac{\varepsilon^i}{\varepsilon_0}\right)^2} \tag{A5}$$

where ε_0 describes the decrease of σ_{sf}^i for non-zero values of ε^i, while ε_1 characterizes the rate of increase of σ_{sf}^i due to stress fiber extension. The strain rate dependency ($f_{\dot{\varepsilon}}$), or velocity-tension relationship of actin-myosin sliding, was described by

$$f_{\dot{\varepsilon}}(\dot{\varepsilon}^i) = \frac{1}{1 + \frac{2}{\sqrt{5}}}\left(1 + \frac{k_{\mathrm{v}}\dot{\varepsilon}^i + 2}{\sqrt{(k_{\mathrm{v}}\dot{\varepsilon}^i + 2)^2 + 1}}\right) \tag{A6}$$

with k_{v} a constant. We refer to Obbink-Huizer et al. (2014) for an extended elaboration on the motivation for these equations.

A.3 Elaboration on determining preferred collagen prestretch

The collagen prestretch algorithm in (12) is determined based on the assumption of equilibrium between the directional stress fiber stress and collagen fiber stress

$$\hat{\sigma}^i_{\mathrm{cf}}(\hat{\lambda}^i_{\mathrm{e}}) = \sigma^i_{\mathrm{sf}}(\lambda^i_{\mathrm{f}}) \qquad \text{(A7)},$$

where $\hat{\sigma}^i_{\mathrm{cf}}$ is the target collagen stress calculated with the target elastic collagen fiber stretch $\hat{\lambda}^i_{\mathrm{e}}$ after inclusion of the prestretch effect. By applying the substitution $\hat{\lambda}^i_{\mathrm{e}} = \frac{\lambda^i_{\mathrm{f}}}{\hat{\lambda}^i_{\mathrm{g}}}$ in the left hand side of (A7), a target inelastic component $\hat{\lambda}^i_{\mathrm{g}}$ in the growth formulation could be derived.

A.4 Mathematical equations for strain-mediated collagen degradation

To model the strain-mediated collagen degradation effect in our model, $f_{\mathrm{deg}}(\varepsilon^i_{\mathrm{e}})$, we followed the continuous functions described by Gaul et al. (2018). Specifically, for the baseline V-shaped strain-mediated collagen degradation curve, the function domain was separated into 3 parts (A8), where $\varepsilon^i_{\mathrm{e}}$ is the elastic collagen strain that follows from the elastic collagen stretch λ^i_{e} by $\varepsilon^i_{\mathrm{e}} = \frac{1}{2}((\lambda^i_{\mathrm{e}})^2 - 1)$. Furthermore, D_{max} is the baseline degradation rate, D_{l} and D_{h} the degradation moduli of the low strain and high strain regions, $\varepsilon_{1,\mathrm{D}}$ the strain where the low strain region switches to the transition region of the curve and $\varepsilon_{2,\mathrm{D}}$ where the curve switches to the high strain region. $T_{1,\mathrm{D}}$, $T_{2,\mathrm{D}}$ and $T_{3,\mathrm{D}}$ are parameters ensuring the continuity between the three strain regions and are defined as

$$\begin{aligned} T_{1,\mathrm{D}} &= (D_{\mathrm{l}} - D_{\mathrm{h}})/(2(\varepsilon_{1,\mathrm{D}} - \varepsilon_{2,\mathrm{D}})) \\ T_{2,\mathrm{D}} &= D_{\mathrm{l}} - \varepsilon_{1,\mathrm{D}}(D_{\mathrm{l}} - D_{\mathrm{h}})/(\varepsilon_{1,\mathrm{D}} - \varepsilon_{2,\mathrm{D}}) \\ T_{3,\mathrm{D}} &= \varepsilon_{1,\mathrm{D}} D_{\mathrm{l}} - \varepsilon^2_{1,\mathrm{D}} T_{1,\mathrm{D}} - \varepsilon_{1,\mathrm{D}} T_{2,\mathrm{D}} \end{aligned} \qquad \text{(A9)}.$$

The parameters $D_{\mathrm{l}}, D_{\mathrm{h}}, \varepsilon_{1,\mathrm{D}}$ and $\varepsilon_{2,\mathrm{D}}$ were effectively fitted to ensure that (1) minimum degradation occurs at the specified transition strain $\varepsilon_{\mathrm{trans}} = \frac{-T_{2,\mathrm{D}}}{2T_{1,\mathrm{D}}}$ and (2) the slope in the high strain regime of the curve passes through a normalized degradation rate of D_{40} for $\varepsilon^i_{\mathrm{e}} = 0.40$ [-] based on the experimental data provided (Ghazanfari et al. 2016). For the mechanobiological variation simulations, a monotonic curve was assumed (Wyatt et al. 2009) where equation (A8) was modified to (A10). In Table 3, the fitted parameter values are reported for different transition strains $\varepsilon_{\mathrm{trans}}$, while keeping D_{max}, D_{min} and D_{40} constant.

Table 3 Variations in strain-mediated collagen degradation curve parameters

Parameter	$\varepsilon_{\mathrm{trans}} = 0.09$	$\varepsilon_{\mathrm{trans}} = 0.18$	$\varepsilon_{\mathrm{trans}} = 0.27$
$\varepsilon_{1,\mathrm{D}}$ [-]	0.083	0.174	0.261
$\varepsilon_{2,\mathrm{D}}$ [-]	0.095	0.186	0.273
D_{max} [-]	1.0	1.0	1.0
D_{min} [-]	0.059	0.059	0.059
D_{40} [-]	0.52	0.52	0.52
D_{l} [-]	−10.57	−5.23	−3.52
D_{h} [-]	1.48	2.10	3.47

A.5 Extended Description Numerical Approximation

The approximation algorithm applied in this study requires the determination of the preferred solution states $\phi^i_{\mathrm{sf,P}}$, $\phi^i_{\mathrm{cf,P}}$ and $\hat{\lambda}^i_{\mathrm{g,P}}$, corresponding to the asymptotic response of the ODE equations under periodic mechanical loading $\varepsilon^i(t)$ (for brevity, this time dependency was omitted in the main text). This section describes the numerical procedure used to obtain these preferred states in more detail. A rigorous mathematical proof of these procedures is extensively described in the source material (Ristori et al. 2016) and only applied in the context of cardiac biomechanics here. It was specifically explained by Ristori et al. (2016) that the periodic solution of the system would approximate an almost constant asymptotic solution for $t \to \infty$. For the evolution of stress fiber volume fractions described in (7), the solution would evolve to a preferred state

$$\begin{aligned} \lim_{t\to+\infty} \phi^i_{\mathrm{sf}} &\approx \frac{1}{T}\int_0^T \tilde{\phi}^i_{\mathrm{sf}}\,\mathrm{d}t \\ &\approx \frac{\bar{a}_i}{\frac{\sum_{j=1}^N \bar{a}_j}{N} + k_{\mathrm{d}}} \phi^{\mathrm{tot}}_{\mathrm{sf}} := \phi^i_{\mathrm{sf,P}} \end{aligned} \qquad \text{(A11)},$$

with $\tilde{\phi}^i_{\mathrm{sf}}$ indicating the periodicity of the asymptotic solution and $\bar{a}_i$ an auxiliary constant capturing the stress fiber reorientation characteristics

$$f_{\mathrm{deg}}(\varepsilon_{\mathrm{e}}^i) = \begin{cases} D_{\max} + \varepsilon_{\mathrm{e}}^i D_{\mathrm{l}} & \text{for } \varepsilon_{\mathrm{e}}^i < \varepsilon_{1,\mathrm{D}} \\ D_{\max} + (\varepsilon_{\mathrm{e}}^i)^2 T_{1,\mathrm{D}} + \varepsilon_{\mathrm{e}}^i T_{2,\mathrm{D}} + T_{3,\mathrm{D}} & \text{for } \varepsilon_{1,\mathrm{D}} \leq \varepsilon_{\mathrm{e}}^i \leq \varepsilon_{2,\mathrm{D}} \\ D_{\max} + (\varepsilon_{\mathrm{e}}^i - \varepsilon_{2,\mathrm{D}}) D_{\mathrm{h}} + \varepsilon_{2,\mathrm{D}}^2 T_{1,\mathrm{D}} + \varepsilon_{2,\mathrm{D}} T_{2,\mathrm{D}} + T_{3,\mathrm{D}} & \text{for } \varepsilon_{\mathrm{e}}^i > \varepsilon_{2,\mathrm{D}} \end{cases} \tag{A8}$$

$$f_{\mathrm{deg}}(\varepsilon_{\mathrm{e}}^i) = \begin{cases} D_{\max} + \varepsilon_{\mathrm{e}}^i D_{\mathrm{l}} & \text{for } \varepsilon_{\mathrm{e}}^i < \varepsilon_{1,\mathrm{D}} \\ D_{\max} + (\varepsilon_{\mathrm{e}}^i)^2 T_{1,\mathrm{D}} + \varepsilon_{\mathrm{e}}^i T_{2,\mathrm{D}} + T_{3,\mathrm{D}} & \text{for } \varepsilon_{1,\mathrm{D}} \leq \varepsilon_{\mathrm{e}}^i \leq \varepsilon_{\mathrm{trans}} \\ D_{\min} & \text{for } \varepsilon_{\mathrm{e}}^i > \varepsilon_{\mathrm{trans}} \end{cases} \tag{A10}$$

averaged over the cardiac cycle period T

$$\begin{aligned} \bar{a}_i &= \frac{1}{T} \int_0^T a_i\big(\varepsilon^i(t), \dot{\varepsilon}^i(t)\big)\, \mathrm{d}t \\ &= \frac{1}{T} \int_0^T (k_0^{\mathrm{f}} + k_1^{\mathrm{f}} \sigma_{\max} f_{\varepsilon,\mathrm{a}}(\varepsilon^i) f_{\dot{\varepsilon}}(\dot{\varepsilon}^i) \\ &\quad + f_{\mathrm{cg}}(\phi_{\mathrm{cf}}^i))\, \mathrm{d}t \end{aligned} \tag{A12}.$$

A forward Riemann's integration scheme was used to numerically determine this integral over the complex periodic signal of cardiac deformations

$$\bar{a}_i \approx \frac{1}{M} \sum_{k=0}^{M-1} a_i\big(\varepsilon^i(t_k), \dot{\varepsilon}^i(t_k)\big) \tag{A13},$$

where M is the number of discrete steps in the Riemann procedure such that each discrete time step $\Delta t = \frac{T}{M}$ and $t_k = k\Delta t$. A value of $M = 100$ was iteratively established to result in convergence of the numerical integration outcomes. Extending on previous implementations (Ristori et al. 2018a,b), the present study applied the approximation algorithm to accurately compute the preferred solution states for collagen volume fraction, $\phi_{\mathrm{cf,P}}^i$, and fibroblast-induced prestretch, $\hat{\lambda}_{\mathrm{g,P}}^i$. For the equation describing evolution of collagen fiber volume fractions while assuming directional fibroblast-mediated production (14), this resulted in a preferred solution

$$\begin{aligned} \lim_{t\to+\infty} \phi_{\mathrm{cf}}^i &\approx \frac{1}{T} \int_0^T \tilde{\phi}_{\mathrm{cf}}^i\, \mathrm{d}t \\ &= \frac{\phi_{\mathrm{cf}}^{\mathrm{tot}}}{\frac{\bar{b}_i}{\bar{A}_i} \sum_{j=1}^N \frac{\bar{A}_j}{\bar{b}_j}} := \phi_{\mathrm{cf,P}}^i \end{aligned} \tag{A14},$$

where $\bar{A}_i$ is a term including the effect of directional fibroblast-mediated production

$$\bar{A}_i = \frac{\frac{1}{T}\int_0^T \tilde{\phi}_{\mathrm{sf}}^i\, \mathrm{d}t}{\sum_{j=1}^N \frac{1}{T}\int_0^T \tilde{\phi}_{\mathrm{sf}}^j\, \mathrm{d}t} \tag{A15},$$

and, $\bar{b}_i$ the auxiliary integral describing collagen degradation

$$\begin{aligned} \bar{b}_i &= \frac{1}{T} \int_0^T b_i\big(\varepsilon_{\mathrm{e}}^i(t)\big)\, \mathrm{d}t \\ &= \frac{1}{T} \int_0^T f_{\mathrm{deg}}\big(\varepsilon_{\mathrm{e}}^i(t)\big)\, \mathrm{d}t \end{aligned} \tag{A16}.$$

When assuming isotropic fibroblast-mediated collagen production, expression (A14) can be simplified since $\bar{A}_i = 1$ to

$$\begin{aligned} \lim_{t\to+\infty} \phi_{\mathrm{cf}}^i &\approx \frac{1}{T} \int_0^T \tilde{\phi}_{\mathrm{cf}}^i\, \mathrm{d}t \\ &= \frac{\phi_{\mathrm{cf}}^{\mathrm{tot}}}{\bar{b}_i \sum_{j=1}^N \frac{1}{\bar{b}_j}} := \phi_{\mathrm{cf,P}}^i \end{aligned} \tag{A17}.$$

Again using Riemann integration, $\bar{b}_i$ and subsequently the solution in (A14) and (A17) were

derived with

$$\bar{b}_i \approx \frac{1}{M} \sum_{k=0}^{M-1} b_i\left(\varepsilon_{\mathrm{e}}^i(t_k)\right) \qquad \text{(A18)}.$$

For the prestretch, the preferred solution simply resembled the temporal average over the periodic input

$$\lim_{t\to+\infty} \hat{\lambda}_{\mathrm{g}}^i \approx \frac{1}{T} \int_0^T \tilde{\hat{\lambda}}_{\mathrm{g}}^i \, \mathrm{d}t = \bar{\hat{\lambda}}_{\mathrm{g}}^i := \hat{\lambda}_{\mathrm{g,P}}^i \qquad \text{(A19)},$$

which was also approximated via numerical integration through

$$\bar{\hat{\lambda}}_{\mathrm{g}}^i \approx \frac{1}{M} \sum_{k=0}^{M-1} \hat{\lambda}_{\mathrm{g}}^i(t_k) \qquad \text{(A20)}.$$

Due to the bidirectional feedback between the solutions for stress fiber volume fractions in (A11) and collagen volume fractions in (A14) and (A17), integral calculations had to be updated over time. An update of the integral every 2400 [s] of simulation time was found to be sufficient to accurately capture this bidirectionality in our system of ODEs.

Supplementary B Results

B.1 Comparison helix angle trajectory with experimental data

In addition to the comparison to the reference alignment of the FE model in Figure 2, we compared the prediction of our numerical framework to *in vivo* measurements in sheep (Walker et al. 2005). The transmural trajectory of collagen fiber helix angles, α_{h}, from the simulations was in agreement with the experimental measurements, $\alpha_{\mathrm{h}}^{\mathrm{exp}}$, showing a clear transmural transition from right-handed endocardial to left-handed epicardial fibers. Furthermore, in both the simulations and the experimental data, differences between helix trajectories at different longitudinal locations are minimal. Some deviations were observed near the endocardial and epicardial surfaces, where the simulations predicted slightly stronger longitudinal fiber orientation than measured experimentally.

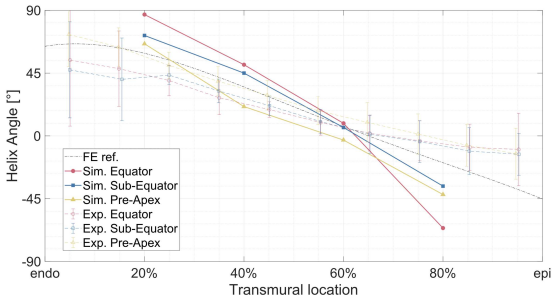


Fig. 7 Resulting collagen helix angles α_{h} from simulations in comparison to experimental measured helix angles $\alpha_{\mathrm{h}}^{\mathrm{exp}}$ in sheep

B.2 Elastic collagen fiber strains in physiological simulations

Here, the fiber strains ε^i shown in Figure 2 are visualized as the corresponding elastic strains, $\varepsilon_{\mathrm{e}}^i$, following the prestretch modification. Because $\varepsilon_{\mathrm{e}}^i$ is defined only for the one-dimensional fiber strain measures, no corresponding elastic fiber strain quantity exists for the circumferential-longitudinal shear strain.

B.3 Supplementary data to variations in strain-dependent degradation

This section provides supplementary data to the results shown in Figure 3. The collagen distribution plots for the variations in V-shaped (Figure 9) and monotonic (Figure 10) strain-mediated degradation are visualized here.

From these distribution plots, it was acknowledged that the results for the V-shaped and monotonic curve for strain-dependent collagen degradation with a lower transition strain $\varepsilon_{\mathrm{trans}} = 0.09$ [-] are more similar to the baseline outcome than the mean collagen fiber angle would suggest (Figure 9a and Figure 10a). Therefore, we performed additional simulations on locations from 5% to 95% on the endo- to epicardium trajectory for these two variations in mechanobiological input parameters and the baseline simulation (Figure 11). Here it is shown how the deviations from the baseline simulations resulted either in unphysiological collagen orientations close to endocardium or close to epicardium for the monotonic curve and V-shaped curve with lower $\varepsilon_{\mathrm{trans}}$ respectively, supporting the results in the main text.

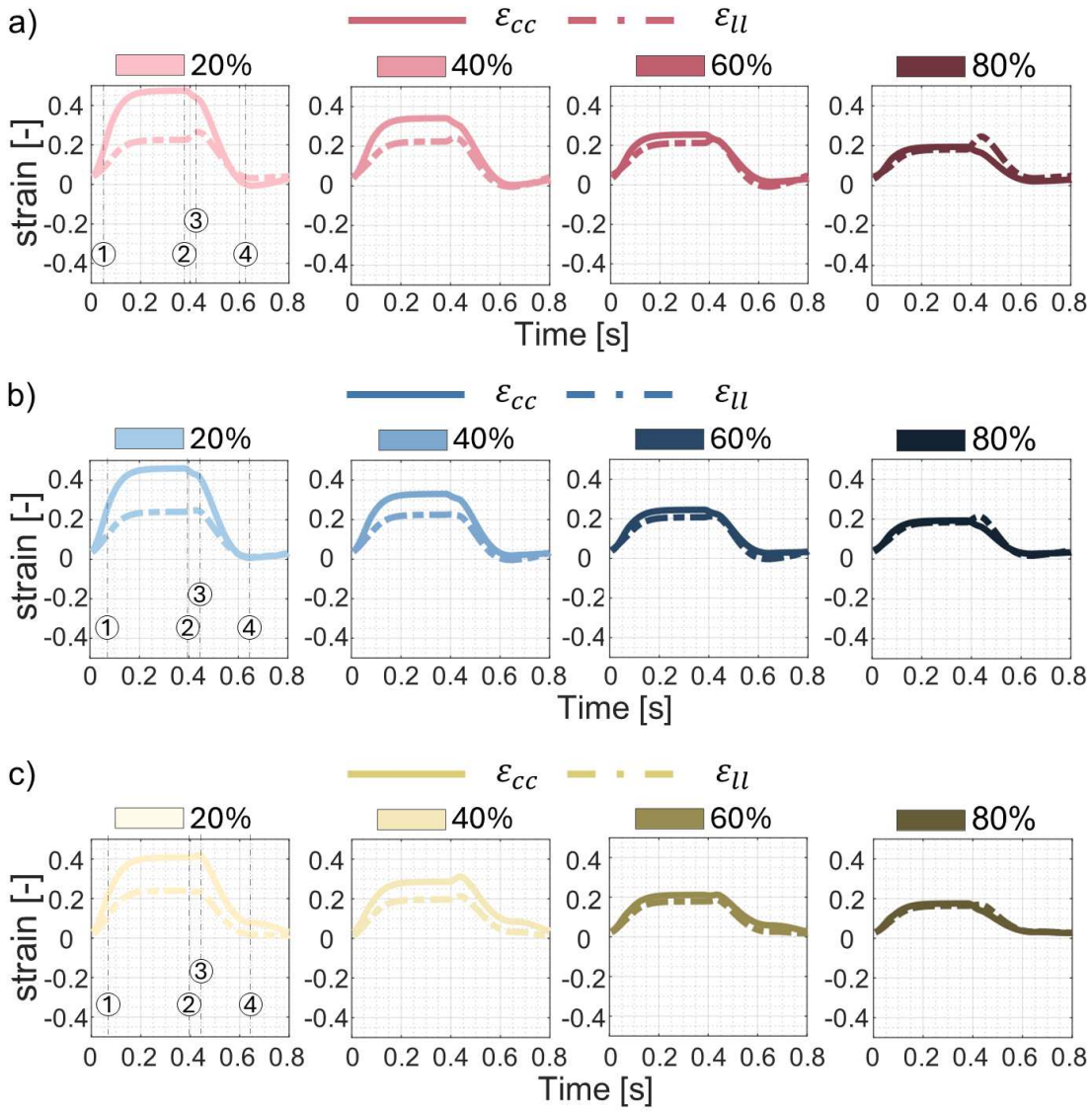


Fig. 8 Elastic collagen strains corrected for fibroblast-mediated prestretch at a) the equator, b) the sub-equator and c) the pre-apex transmural locations

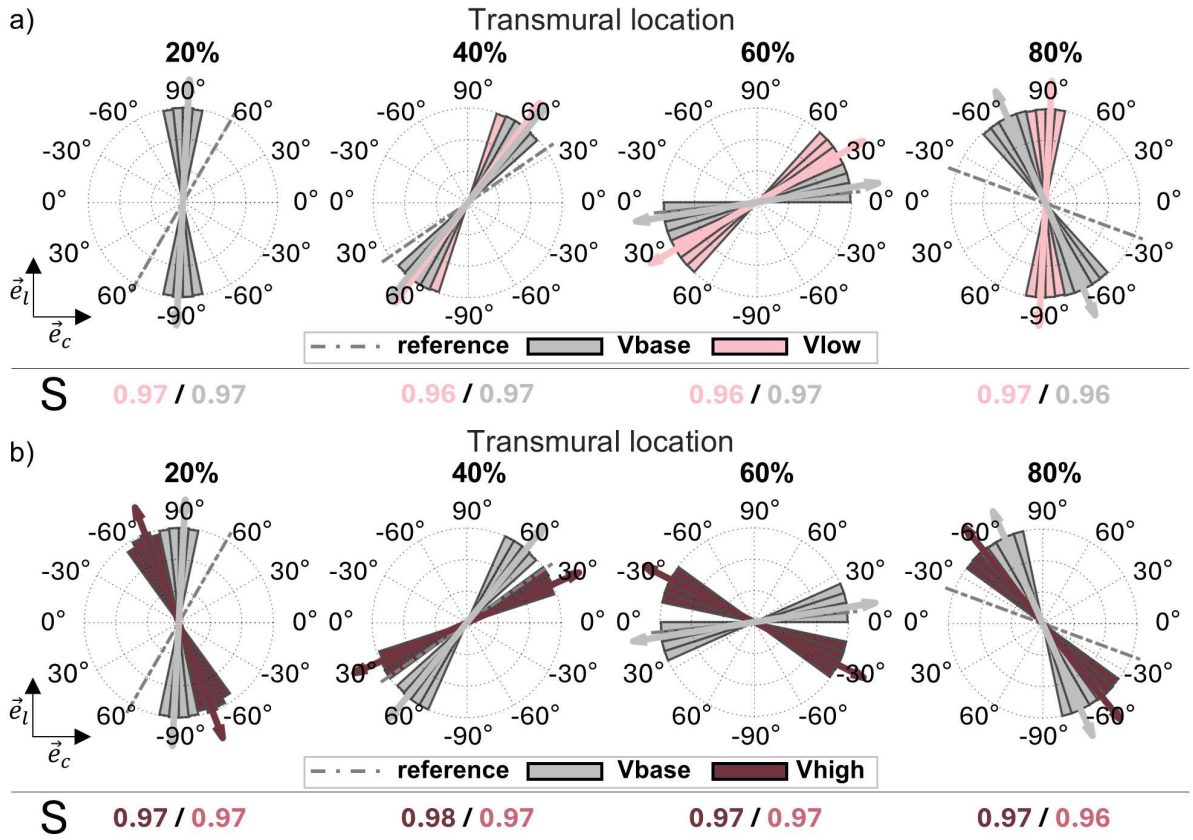


Fig. 9 Collagen volume fractions for variations in V-shaped strain-mediated degradation curve

B.4 Supplementary data to variations in stress fiber contractility $\sigma_{\max}$

This section provides supplementary data to the results shown in Figure 5. The collagen distribution plots for the variations in maximum stress fiber contractility $\sigma_{\max}$ are visualized here (Figure 12).

References

Arts T, Prinzen FW, Snoeckx LH, et al (1994) Adaptation of cardiac structure by mechanical feedback in the environment of the cell: a model study. Biophysical Journal 66(4):953–961. https://doi.org/10.1016/S0006-3495(94)80876-8

Atance J, Yost MJ, Carver W (2004) Influence of the extracellular matrix on the regulation of cardiac fibroblast behavior by mechanical stretch. Journal of Cellular Physiology 200(3):377–386. https://doi.org/10.1002/jcp.20034

Atluri K, Chinnathambi S, Mendenhall A, et al (2020) Targeting cell contractile forces: a novel minimally invasive treatment strategy for fibrosis. Annals of Biomedical Engineering 48(6):1850–1862. https://doi.org/10.1007/s10439-020-02497-x

Bai Y, Lee PF, Humphrey JD, et al (2014) Sequential multimodal microscopic imaging and biaxial mechanical testing of living multicomponent tissue constructs. Annals of Biomedical Engineering 42(9):1791–1805. https://doi.org/10.1007/s10439-014-1019-3

Baratta IA, Dean JP, Dokken JS, et al (2023) DOLFINx: the next generation FEniCS problem solving environment. https://doi.org/10.5281/zenodo.10447666

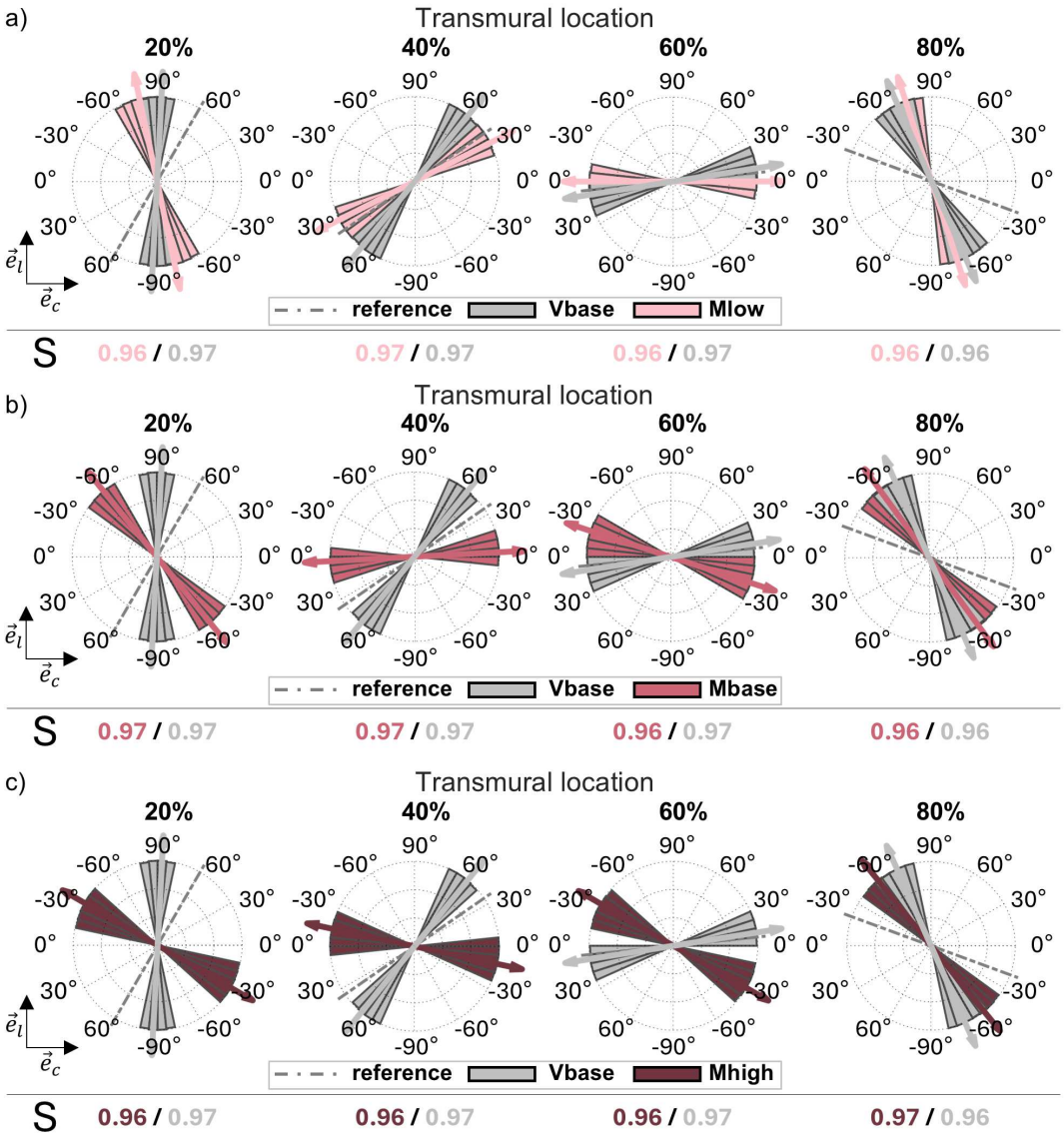


Fig. 10 Collagen volume fractions for variations in monotonic strain-mediated degradation curve

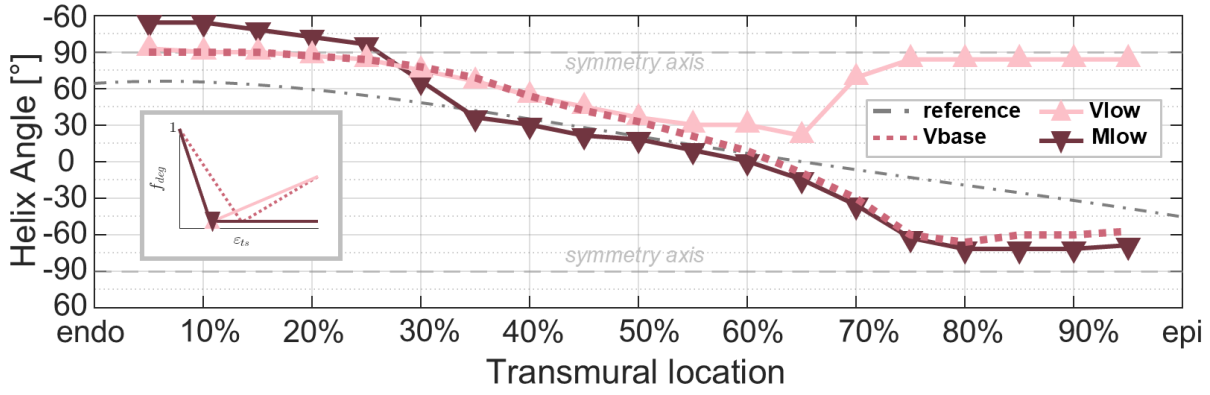


Fig. 11 Additional simulations on various transmural locations for relevant strain-dependent collagen degradation curve variations

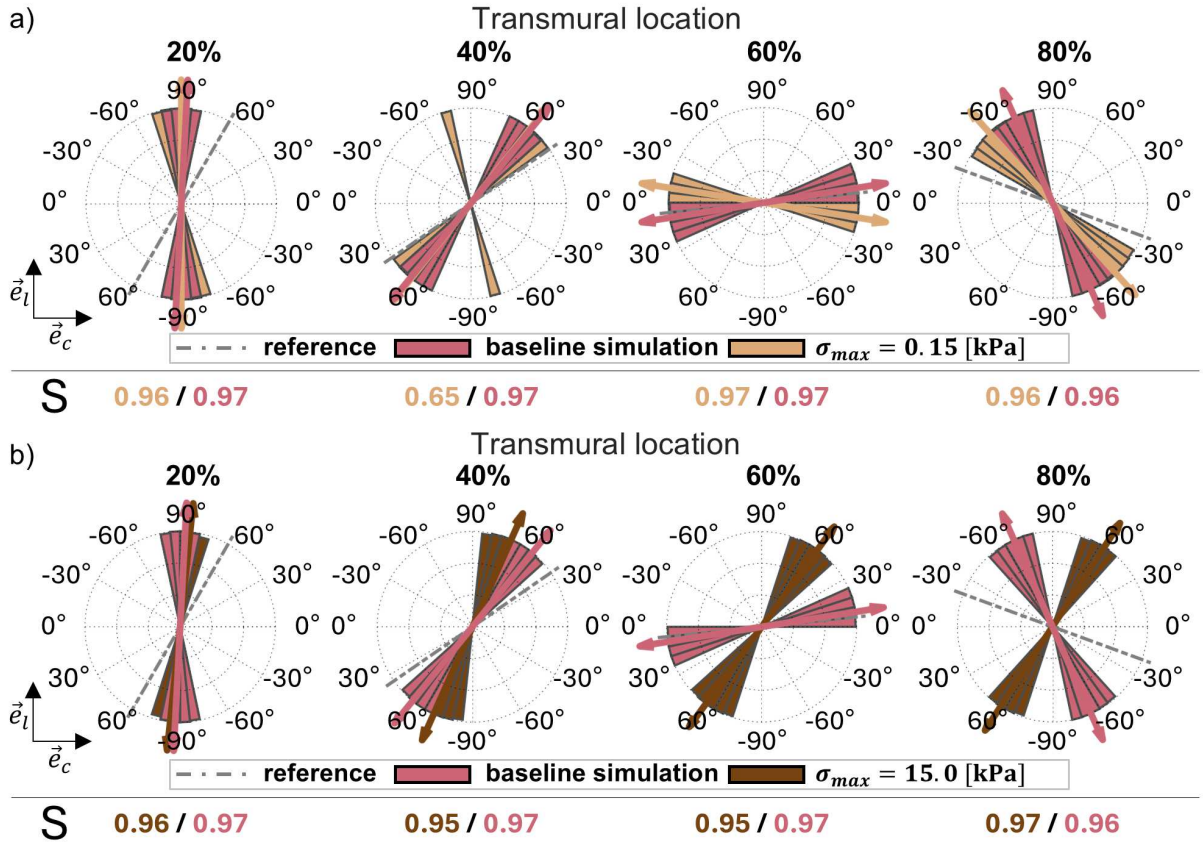


Fig. 12 Collagen volume fractions for variations in maximum stress fiber contractility $\sigma_{\max}$

Barbarotta L, Bovendeerd PHM (2021) A computational approach on sensitivity of left ventricular wall strains to fiber orientation. In: Ennis DB, Perotti LE, Wang VY (eds) Functional Imaging and Modeling of the Heart, Lecture Notes in Computer Science, vol 12738. Springer International Publishing, Cham, p 296–304, https://doi.org/10.1007/978-3-030-78710-3_29

Barbour K, Huang HYS (2020) Strain effects on collagen proteolysis in heart valve tissues. Mechanics of Time-Dependent Materials 24(1):85–100. https://doi.org/10.1007/s11043-019-09410-7

Bishop JE (1998) Regulation of cardiovascular collagen deposition by mechanical forces. Molecular Medicine Today 4(2):69–75. https://doi.org/10.1016/S1357-4310(97)01193-3

Bovendeerd PHM, Kroon W, Delhaas T (2009) Determinants of left ventricular shear strain. American Journal of Physiology-Heart and Circulatory Physiology 297(3):H1058–H1068. https://doi.org/10.1152/ajpheart.01334.2008

Braidotti N, Demontis G, Conti M, et al (2024) The local mechanosensitive response of primary cardiac fibroblasts is influenced by the microenvironment mechanics. Scientific Reports 14(1):10365. https://doi.org/10.1038/s41598-024-60685-4

Brilla CG, Rupp H, Funck R, et al (1995) The renin-angiotensin-aldosterone system and myocardial collagen matrix remodelling in congestive heart failure. European Heart Journal 16(Suppl O):107–109. https://doi.org/10.1093/eurheartj/16.suppl_O.107

Carruth ED, McCulloch AD, Omens JH (2016) Transmural gradients of myocardial structure and mechanics: implications for fiber stress and strain in pressure overload. Progress in Biophysics and Molecular Biology 122(3):215–226. https://doi.org/10.1016/j.pbiomolbio.2016.11.004

Dassault Systèmes Simulia Corp. (2024) Abaqus/Standard. Dassault Systèmes, Johnston, RI, USA, version 2024

Deng Y, Herrmann J, Wang Y, et al (2024) Physiological mechanical forces accelerate the degradation of bovine lung collagen fibers by bacterial collagenase. Scientific Reports 14(1):29008. https://doi.org/10.1038/s41598-024-77704-z

Deshpande VS, McMeeking RM, Evans AG (2006) A bio-chemo-mechanical model for cell contractility. Proceedings of the National Academy of Sciences 103(38):14015–14020. https://doi.org/10.1073/pnas.0605837103

Fomovsky GM, Rouillard AD, Holmes JW (2012) Regional mechanics determine collagen fiber structure in healing myocardial infarcts. Journal of Molecular and Cellular Cardiology 52(5):1083–1090. https://doi.org/10.1016/j.yjmcc.2012.02.012

Foolen J, Deshpande VS, Kanters FMW, et al (2012) The influence of matrix integrity on stress-fiber remodeling in 3D. Biomaterials 33(30):7508–7518. https://doi.org/10.1016/j.biomaterials.2012.06.103

Gaul RT, Nolan DR, Ristori T, et al (2018) Strain mediated enzymatic degradation of arterial tissue: insights into the role of the non-collagenous tissue matrix and collagen crimp. Acta Biomaterialia 77:301–310. https://doi.org/10.1016/j.actbio.2018.06.037

Ghazanfari S, Driessen-Mol A, Bouten CVC, et al (2016) Modulation of collagen fiber orientation by strain-controlled enzymatic degradation. Acta Biomaterialia 35:118–126. https://doi.org/10.1016/j.actbio.2016.02.033

Gould RA, Chin K, Santisakultarm TP, et al (2012) Cyclic strain anisotropy regulates valvular interstitial cell phenotype and tissue remodeling in 3D culture. Acta Biomaterialia 8(5):1710–1719. https://doi.org/10.1016/j.actbio.2012.01.006

Greiner J, Sankarankutty AC, Seemann G, et al (2018) Confocal microscopy-based estimation of parameters for computational modeling of electrical conduction in the normal and infarcted heart. Frontiers in Physiology 9:239. https://doi.org/10.3389/fphys.2018.00239

Guan D, Luo X, Gao H (2025) Constrained mixture models of growth and remodelling in an infarct left ventricle: a modelling study. Journal of the Mechanics and Physics of Solids 200:106121. https://doi.org/10.1016/j.jmps.2025.106121

Guido S, Tranquillo RT (1993) A methodology for the systematic and quantitative study of cell contact guidance in oriented collagen gels: correlation of fibroblast orientation and gel birefringence. Journal of Cell Science 105(2):317–331. https://doi.org/10.1242/jcs.105.2.317

Gupta KB, Ratcliffe MB, Fallert MA, et al (1994) Changes in passive mechanical stiffness of myocardial tissue with aneurysm formation. Circulation 89(5):2315–2326. https://doi.org/10.1161/01.cir.89.5.2315

Hermans LHL (2024) Mechanobiology of the myocardial infarct border zone in vitro: a quantitative analysis. PhD thesis, Eindhoven University of Technology

Hervas A, Ruiz-Sauri A, De Dios E, et al (2016) Inhomogeneity of collagen organization within the fibrotic scar after myocardial infarction: results in a swine model and in human samples. Journal of Anatomy 228(1):47–58. https://doi.org/10.1111/joa.12395

Huang C, Yannas IV (1977) Mechanochemical studies of enzymatic degradation of insoluble collagen fibers. Journal of Biomedical Materials Research 11(1):137–154. https://doi.org/10.1002/jbm.820110113

Humphrey JD, Rajagopal KR (2002) A constrained mixture model for growth and remodeling of soft tissues. Mathematical Models and Methods in Applied Sciences 12(3):407–430. https://doi.org/10.1142/S0218202502001714

Janssens KLPM, Kraamer M, Barbarotta L, et al (2023) Post-infarct evolution of ventricular and myocardial function. Biomechanics and Modeling in Mechanobiology 22(6):1815–1828. https://doi.org/10.1007/s10237-023-01734-1

Jenkins TL, Darden K, Pourdeyhimi B, et al (2026) Dynamic tensile loading improves neotendon formation at moderate daily loading cycles, but impairs neotendon formation at high daily loading cycles. Journal of Biomechanics 201:113248. https://doi.org/10.1016/j.jbiomech.2026.113248

de Jonge N, Kanters FMW, Baaijens FPT, et al (2013) Strain-induced collagen organization at the micro-level in fibrin-based engineered tissue constructs. Annals of Biomedical Engineering 41(4):763–774. https://doi.org/10.1007/s10439-012-0704-3

Kluge JA, Thurber A, Leisk GG, et al (2010) A model for the stretch-mediated enzymatic degradation of silk fibers. Journal of the Mechanical Behavior of Biomedical Materials 3(7):538–547. https://doi.org/10.1016/j.jmbbm.2010.06.008

Kroon W, Delhaas T, Bovendeerd PHM, et al (2009) Computational analysis of the myocardial structure: adaptation of cardiac myofiber orientations through deformation. Medical Image Analysis 13(2):346–353. https://doi.org/10.1016/j.media.2008.06.015

Loerakker S, Argento G, Oomens CWJ, et al (2013) Effects of valve geometry and tissue anisotropy on the radial stretch and coaptation area of tissue-engineered heart valves. Journal of Biomechanics 46(11):1792–1800. https://doi.org/10.1016/j.jbiomech.2013.05.015

Loerakker S, Obbink-Huizer C, Baaijens FPT (2014) A physically motivated constitutive model for cell-mediated compaction and collagen remodeling in soft tissues. Biomechanics and Modeling in Mechanobiology 13(5):985–1001. https://doi.org/10.1007/s10237-013-0549-1

McEvoy E, Deshpande VS, McGarry P (2019) Transient active force generation and stress fibre remodelling in cells under cyclic loading. Biomechanics and Modeling in Mechanobiology 18(4):921–937. https://doi.org/10.1007/s10237-019-01121-9

Mehri M, Wenk JF (2026) A unified finite element framework for cardiac growth and remodeling in mitral regurgitation incorporating fiber reorientation and baroreflex. Acta Biomaterialia 210:110–120. https://doi.org/10.1016/j.actbio.2025.12.012

Mehri M, Sharifi H, Mann CK, et al (2024) Multiscale fiber remodeling in the infarcted left ventricle using a stress-based reorientation law. Acta Biomaterialia 189:337–350. https://doi.org/10.1016/j.actbio.2024.09.049

Mehri M, Campbell KS, Lee LC, et al (2025) A multi-scale finite element method for investigating fiber remodeling in hypertrophic cardiomyopathy. Scientific Reports 15(1):31961. https://doi.org/10.1038/s41598-025-17778-5

Meshel AS, Wei Q, Adelstein RS, et al (2005) Basic mechanism of three-dimensional collagen fibre transport by fibroblasts. Nature Cell Biology 7(2):157–164. https://doi.org/10.1038/ncb1216

Mostert D, Groenen B, Klouda L, et al (2022) Human pluripotent stem cell-derived cardiomyocytes align under cyclic strain when guided by cardiac fibroblasts. APL Bioengineering 6(4):046108. https://doi.org/10.1063/5.0108914

Mostert D, Van Der Putten C, Sahlgren CM, et al (2025) Bioengineering structural anisotropy in living tissues. Nature Reviews Bioengineering https://doi.org/10.1038/s44222-025-00338-x

Mostert D, Hoursan H, Goumans MJTH, et al (2026) Restoration of structural organization in engineered cardiac microtissues is promoted by cardiomyocyte beating. Communications Biology 9:1029. https://doi.org/10.1038/s42003-026-10121-2

Moulin K, Croisille P, Viallon M, et al (2021) Myofiber strain in healthy humans using DENSE and cDTI. Magnetic Resonance in Medicine 86(1):277–292. https://doi.org/10.1002/mrm.28724

Nguyen TD, Liang R, Woo SLY, et al (2009) Effects of cell seeding and cyclic stretch on the fiber remodeling in an extracellular matrix–derived bioscaffold. Tissue Engineering Part A 15(4):957–963. https://doi.org/10.1089/ten.tea.2007.0384

Obbink-Huizer C, Oomens CWJ, Loerakker S, et al (2014) Computational model predicts cell orientation in response to a range of mechanical stimuli. Biomechanics and Modeling in Mechanobiology 13(1):227–236. https://doi.org/10.1007/s10237-013-0501-4

Papazafeiropoulos G, Muñiz-Calvente M, Martínez-Pañeda E (2017) Abaqus2matlab: A suitable tool for finite element post-processing. Advances in Engineering Software 105:9–16. https://doi.org/10.1016/j.advengsoft.2017.01.006

Pereira-Sousa D, Guillamat P, Niro F, et al (2026) Cardiac fibroblast anisotropy is determined by YAP-dependent cellular contractility and ECM production. Biomaterials 333:124205. https://doi.org/10.1016/j.biomaterials.2026.124205

Pesce M, Duda GN, Forte G, et al (2023) Cardiac fibroblasts and mechanosensation in heart development, health and disease. Nature Reviews Cardiology 20(5):309–324. https://doi.org/10.1038/s41569-022-00799-2

Pope AJ, Sands GB, Smaill BH, et al (2008) Three-dimensional transmural organization of perimysial collagen in the heart. American Journal of Physiology-Heart and Circulatory Physiology 295(3):H1243–H1252. https://doi.org/10.1152/ajpheart.00484.2008

Richardson WJ, Holmes JW (2016) Emergence of collagen orientation heterogeneity in healing infarcts and an agent-based model. Biophysical Journal 110(10):2266–2277. https://doi.org/10.1016/j.bpj.2016.04.014

Richardson WJ, Kegerreis B, Thomopoulos S, et al (2018) Potential strain-dependent mechanisms defining matrix alignment in healing tendons. Biomechanics and Modeling in Mechanobiology 17(6):1569–1580. https://doi.org/10.1007/s10237-018-1044-5

Ristori T, Obbink-Huizer C, Oomens CWJ, et al (2016) Efficient computational simulation of actin stress fiber remodeling. Computer Methods in Biomechanics and Biomedical Engineering 19(12):1347–1358. https://doi.org/10.1080/10255842.2016.1140748

Ristori T, Bouten CVC, Baaijens FPT, et al (2018a) Predicting and understanding collagen remodeling in human native heart valves during early development. Acta Biomaterialia 80:203–216. https://doi.org/10.1016/j.actbio.2018.08.040

Ristori T, Notermans TMW, Foolen J, et al (2018b) Modelling the combined effects of collagen and cyclic strain on cellular orientation in collagenous tissues. Scientific Reports 8(1):8518. https://doi.org/10.1038/s41598-018-26989-y

Rouillard AD, Holmes JW (2014) Coupled agent-based and finite-element models for predicting scar structure following myocardial infarction. Progress in Biophysics and Molecular Biology 115(2):235–243. https://doi.org/10.1016/j.pbiomolbio.2014.06.010

Saez A, Ghibaudo M, Buguin A, et al (2007) Rigidity-driven growth and migration of epithelial cells on microstructured anisotropic substrates. Proceedings of the National Academy of Sciences 104(20):8281–8286. https://doi.org/10.1073/pnas.0702259104

Shinde AV, Humeres C, Frangogiannis NG (2017) The role of alpha-smooth muscle actin in fibroblast-mediated matrix contraction and remodeling. Biochimica et Biophysica Acta (BBA) - Molecular Basis of Disease 1863(1):298–309. https://doi.org/10.1016/j.bbadis.2016.11.006

Simpson DG, Terracio L, Terracio M, et al (1994) Modulation of cardiac myocyte phenotype in vitro by the composition and orientation of the extracellular matrix. Journal of Cellular Physiology 161(1):89–105. https://doi.org/10.1002/jcp.1041610112

Spinale FG (2007) Myocardial matrix remodeling and the matrix metalloproteinases: influence on cardiac form and function. Physiological Reviews 87(4):1285–1342. https://doi.org/10.1152/physrev.00012.2007

The MathWorks Inc. (2023) Matlab version: 9.14.0 (r2023a). https://www.mathworks.com

Uiterwijk M, Smits AIPM, van Geemen D, et al (2020) In situ remodeling overrules bioinspired scaffold architecture of supramolecular elastomeric tissue-engineered heart valves. JACC: Basic to Translational Science 5(12):1187–1206. https://doi.org/10.1016/j.jacbts.2020.09.011

Vernerey FJ, Farsad M (2011) A constrained mixture approach to mechano-sensing and force generation in contractile cells. Journal of the Mechanical Behavior of Biomedical Materials 4(8):1683–1699. https://doi.org/10.1016/j.jmbbm.2011.05.022

Vigliotti A, Ronan W, Baaijens FPT, et al (2016) A thermodynamically motivated model for stress-fiber reorganization. Biomechanics and Modeling in Mechanobiology 15(4):761–789. https://doi.org/10.1007/s10237-015-0722-9

Visser VL, Motta SE, Hoerstrup SP, et al (2025) Smooth leaflets with curved belly and attachment edge profiles promote adaptive remodeling in tissue-engineered heart valves: an in silico study. Biomechanics and Modeling in Mechanobiology 24:811–828. https://doi.org/10.1007/s10237-025-01937-8

van Vlimmeren MAA, Driessen-Mol A, Oomens CWJ, et al (2012) Passive and active contributions to generated force and retraction in heart valve tissue engineering. Biomechanics and Modeling in Mechanobiology 11(7):1015–1027. https://doi.org/10.1007/s10237-011-0370-7

Walker JC, Guccione JM, Jiang Y, et al (2005) Helical myofiber orientation after myocardial infarction and left ventricular surgical restoration in sheep. The Journal of Thoracic and Cardiovascular Surgery 129(2):382–390. https://doi.org/10.1016/j.jtcvs.2004.06.006

Wang JHC, Grood ES (2000) The strain magnitude and contact guidance determine orientation response of fibroblasts to cyclic substrate strains. Connective Tissue Research 41(1):29–36. https://doi.org/10.3109/03008200009005639

Wang VY, Casta C, Zhu YM, et al (2016) Image-based investigation of human in vivo myofibre strain. IEEE Transactions on Medical Imaging 35(11):2486–2496. https://doi.org/10.1109/TMI.2016.2580573

Washio T, Yoneda K, Okada J.-i, et al (2016) Ventricular fiber optimization utilizing the branching structure. International Journal for Numerical Methods in Biomedical Engineering 32(7):e02753. https://doi.org/10.1002/cnm.2753

Washio T, Sugiura S, Okada J.-i, et al (2020) Using systolic local mechanical load to predict fiber orientation in ventricles. Frontiers in Physiology 11:467. https://doi.org/10.3389/fphys.2020.00467

Weber KT (1989) Cardiac interstitium in health and disease: the fibrillar collagen network. Journal of the American College of Cardiology 13(7):1637–1652. https://doi.org/10.1016/0735-1097(89)90360-4

Weber KT, Brilla CG (1991) Pathological hypertrophy and cardiac interstitium: fibrosis and renin-angiotensin-aldosterone system. Circulation 83(6):1849–1865. https://doi.org/10.1161/01.CIR.83.6.1849

Weber KT, Sun Y, Tyagi SC, et al (1994) Collagen network of the myocardium: function, structural remodeling and regulatory mechanisms. Journal of Molecular and Cellular Cardiology 26(3):279–292. https://doi.org/10.1006/jmcc.1994.1036

Weinberger F, Breckwoldt K, Pecha S, et al (2016) Cardiac repair in guinea pigs with human engineered heart tissue from induced pluripotent stem cells. Science Translational Medicine 8(363):363ra148. https://doi.org/10.1126/scitranslmed.aaf8781

Williams NP, Beussman KM, Foster JR, et al (2025) Bioengineered human cardiac ventricular model with transmural helical remodeling. Advanced Healthcare Materials 14(22):2502005. https://doi.org/10.1002/adhm.202502005

Wu Y, Tse HF, Wu EX (2006) Diffusion tensor MRI study of myocardium structural remodeling after infarction in porcine model. In: 28th Annual International Conference of the IEEE Engineering in Medicine and Biology Society. IEEE, New York, NY, USA, pp 1069–1072, https://doi.org/10.1109/IEMBS.2006.259840

Wyatt KEK, Bourne JW, Torzilli PA (2009) Deformation-dependent enzyme mechanokinetic cleavage of type I collagen. Journal of Biomechanical Engineering 131(5):051004. https://doi.org/10.1115/1.3078177

Yang S, Valencia FR, Sabass B, et al (2021) Quantitative analysis of myofibroblast contraction by traction force microscopy. In: Hinz B, Lagares D (eds) Myofibroblasts: Methods and Protocols, Methods in Molecular Biology, vol 2299. Humana, New York, NY, p 181–195, https://doi.org/10.1007/978-1-0716-1382-5_14

Yeganegi A, Whitehead K, De Castro Brás LE, et al (2023) Mechanical strain modulates extracellular matrix degradation and byproducts in an isoform-specific manner. Biochimica et Biophysica Acta (BBA) - General Subjects 1867(3):130286. https://doi.org/10.1016/j.bbagen.2022.130286

Yi E, Sato S, Takahashi A, et al (2016) Mechanical forces accelerate collagen digestion by bacterial collagenase in lung tissue strips. Frontiers in Physiology 7:287. https://doi.org/10.3389/fphys.2016.00287

Younesi FS, Miller AE, Barker TH, et al (2024) Fibroblast and myofibroblast activation in normal tissue repair and fibrosis. Nature Reviews Molecular Cell Biology 25(8):617–638. https://doi.org/10.1038/s41580-024-00716-0

Zhuan X, Luo X, Gao H, et al (2019) Coupled agent-based and hyperelastic modelling of the left ventricle post-myocardial infarction. International Journal for Numerical Methods

in Biomedical Engineering 35(1):e3155. https://doi.org/10.1002/cnm.3155